Aus der Klinik für Kardiologie und Pneumologie
(Prof. Dr. med. G. Hasenfuß)
der Medizinischen Fakultät der Universität Göttingen

Involvement of cardiac fibroblasts in anthracycline-induced cardiotoxicity

INAUGURAL-DISSERTATION

zur Erlangung des Doktorgrades
der Medizinischen Fakultät der
Georg-August-Universität zu Göttingen

vorgelegt von

Steffen Köhne

aus Hamburg

Göttingen 2021

Dekan:	Prof. Dr. med. W. Brück

Betreuungsausschuss

Betreuerin:	Prof. Dr. rer. nat. K. Streckfuß-Bömeke
Ko-Betreuer:	Prof. Dr. mult. T. Meyer

Prüfungskommission

Referent/in	Prof. Dr. rer. nat. K. Streckfuß-Bömeke
Ko-Referent/in:	Prof. Dr. mult. T. Meyer
Drittreferent/in:	Prof. Dr. med. Ralf Dressel

Datum der mündlichen Prüfung: 26.10.2021

Hiermit erkläre ich, die Dissertation mit dem Titel "Involvement of cardiac fibroblasts in anthracycline-induced cardiotoxicity" eigenständig angefertigt und keine anderen als die von mir angegebenen Quellen und Hilfsmittel verwendet zu haben.

Göttingen, den …… ……

(Unterschrift)

Die Daten, auf denen die vorliegende Arbeit basiert, wurden teilweise publiziert:

Hübscher D, Rebs S, Haupt L, Borchert T, Guessoum CI, Treu F, **Köhne S**, Maus A, Hambrecht M, Sossalla S, et al. (2019): A High-Throughput Method as a Diagnostic Tool for HIV Detection in Patient-Specific Induced Pluripotent Stem Cells Generated by Different Reprogramming Methods. Stem Cells Int 2019, 2181437

Köhne S, Haupt L, Seguin M, Wojnowski L, Dressel R, Sossalla S, Hasenfuss G, Streckfuss-Boemeke K (2017): Comparative study of human iPSC- cardiomyocytes, human cardiac fibroblasts, and adult cardiac tissue of anthracyclin-induced cardiotoxicity patients. Vortrag im Rahmen der 83. Jahrestagung der Deutschen Gesellschaft für Kardiologie, Mannheim, 19.04. – 22.04.2017.

Köhne S, Haupt L, Sossalla S, Hasenfuss G, Streckfuss-Boemke K (2018): Role of cardiac fibroblasts in anthracycline-induced cardiotoxicity. Posterpräsentation im Rahmen des 16. German-Dutch-Meeting of the Molecular Cardiology Working Groups, Amsterdam, 15.03. – 17.03.2018.

Table of contents

List of figures

List of tables

List of abbreviations

ACT	Anthracycline-induced cardiotoxicity
ANOVA	Analysis of variance
BSA	Bovine serum albumin
cDNA	Complementary DNA
cFB	Cardiac fibroblasts
COL1A1	Collagen 1A1
CTGF	Connective tissue growth factor
CYBA	Cytochrome B-245 alpha chain
DAPI	4', 6-Diamidino-2-phenylindole dihydrochloride
DCM	Dilative cardiomyopathy
dH_2O	Deionized water
DHE	Dihydroethidium
DMEM	Dulbecco's modified Eagle medium
DOX	Doxorubicin
SF	Skin fibroblasts
DPBS	Dulbecco's phosphate-buffered saline
DTT	Dithiothreitol
ECM	Extracellular matrix
FBS	Fetal bovine serum
FSP-1	Fibroblast-specific protein 1
GAPDH	Glyceraldehyde-3-phosphate dehydrogenase
H_2O_2	Hydrogen peroxide
hbFGF	Recombinant human basic fibroblast growth factor
HCl	Hydrochloric acid
HFBM	Human fibroblast medium
HPLC	High-performance liquid chromatography
HRP	Horseradish peroxidase
KCl	Potassium chloride
LVEF	Left ventricular ejection fraction
$MgCl_2$	Magnesium chloride
MMP2	Matrix metalloproteinase-2
MMP9	Matrix metalloproteinase-9
MRI	Magnetic resonance imaging
mRNA	Messenger RNA
Na_3VO_4	Sodium orthovanadate
NaCl	Sodium chloride
NADPH	Nicotinamide adenine dinucleotide phosphate

NaF	Sodium fluoride
NCF1	Neutrophil cytosolic factor 1
NCF2	Neutrophil cytosolic factor 2
NCF4	Neutrophil cytosolic factor 4
NEAA	Non-essential amino acids
NF	Non-failing
PFA	Paraformaldehyde
PLN	Phospholamban
qRT-PCR	Quantitive real-time polymerase chain reaction
RAC1	Ras-related C3 botulinum toxin substrate 1
RAC2	Ras-related C3 botulinum toxin substrate 2
ROS	Reactive oxygen species
rpm	Rounds per minute
SDS	Sodium dodecyl sulfate
SEM	Standard error of mean
SERCA	Sarco/Endoplasmic reticulum Ca^{2+}-ATPase
SERCA2a	Sarco/Endoplasmic reticulum Ca^{2+}-ATPase 2a
SNP	Single nucleotid polymorphism
SOD	Superoxide dismutase
ß-ME	ß-Mercaptoethanol
T/E	Trypsin/EDTA
TCF21	Transcription factor 21
TEMED	Tetramethylethylenediamine
TOP1mt	Mitochondrial topoisomerase I
TOP2	Topoisomerase II
α-SMA	α-smooth muscle actin

1 Introduction

1.1 Anthracycline-induced cardiotoxicity

1.1.1 Anthracyclines

Anthracyclines are a group of antibiotic chemotherapy drugs that were isolated from *Streptomyces peucetius* for the first time in the 1960s (Arcamone et al. 1969). The World Health Organization lists anthracyclines, like doxorubicin and daunorubicin, in its Model List of Essential Medicines for the treatment of various hematological and solid tumors including common neoplasias like breast cancer, lymphomas and leukemia in adults and children (World Health Organization 2017).

With one out of three people in first world countries being affected by cancer (Siegel. et al. 2018) and increasing survival rates due to improved therapy regimen (Coleman et al. 2011), the number of people with an anthracycline treatment in their medical history will grow.

1.1.2 Cardiotoxicity

The clinical use of anthracyclines is limited because of an adverse effect. The momentous side-effect highly impairing patient outcome is the cardiotoxicity first described in the 1970s (Middleman et al. 1971; Von Hoff 1979). Currently, there is no clear definition of anthracycline-induced cardiotoxicity (ACT), but the disease has been categorized based on the time after treatment at which cardiac effects occur into acute, early-onset and late-onset ACT (Tan et al. 2015). While the acute form appears to be pathologically independent, early-onset and late-onset ACT seem to belong to a single disease manifestation process resulting in chronic ACT (McGowan et al. 2017).

Acute ACT occurs within the first hours or days after treatment. Clinically, patients present electrocardiographic abnormalities such as QT-interval changes, arrhythmias, different heart blocks or repolarization irregularities, ventricular dysfunction with a decrease of left ventricular ejection fraction (LVEF) and/or myocarditis-pericarditis syndrome (Gaudin et al. 1993; Singal 1998; Kilickap et al. 2005; Guglin et al. 2009). It is relatively benign and reversible with the discontinuation of chemotherapy. Incidence rates are highly variable due to the unclear definition of acute ACT, but generally low when compared to the other forms of ACT (Tan et al. 2015).

Chronic ACT, often split into early-onset and late-onset, is defined as a cumulative, dose-dependent form of congestive heart failure resulting in a clinical presentation ranging from subclinical ventricular dysfunction to end-stage heart failure (Rahman et al. 2007). The consensus diagnosis of chronic ACT has been described as a decrease in LVEF of more than 10 points or <50 % (Ganz et al. 1993) with a highly variable latent period between anthracycline treatment and ACT manifestation of months to even decades (Steinherz et al. 1991). Histopathological damage includes myofibril loss, increase in cardiomyocyte apoptosis and cardiac fibrosis (Unverferth et al. 1983; Doroshow et al. 1985), which leads to a degeneration of the left ventricle and the manifestation as a dilative cardiomyopathy (Carvalho et al. 2014). The incidence of chronic ACT is mainly influenced by the cumulative dosage of doxorubicin (DOX) or other anthracyclines. Retrospective studies reported symptomatic heart failure in 7 to 26 % of all patients treated with 550 mg/m^2 DOX and 18 to 48 % of patients treated with 700 mg/m^2 DOX (Von Hoff 1979; Swain et al. 2003). Consequently, the lifetime cumulative doxorubicin-equivalent exposure was limited to 450 mg/m^2 (McGowan et al. 2017). Still, recent studies following patients with suggested doses found symptomatic heart failure in 6 to 9 % of all cases (Lotrionte et al. 2013; Cardinale et al. 2015). Further risk factors include pre-existing cardiac diseases, hypertension, age over 65 years or under 5 years, hyperlipidemia and mediastinal radiation therapy (Singal 1998; Kremer et al. 2002; Doyle et al. 2005).

As lowering of treatment intensity means a decrease in chemotherapeutic potency, the search for prophylactic and/or therapeutic options is crucial for improving patient outcome.

1.1.3 Prevention and therapy

The search for cardioprotective measures against ACT has yielded little success so far. Various studied agents like carvedilol, valsartan, co-enzyme Q10, carnitine, n-acetylcysteine and vitamins A, C and E show inconclusive effectiveness in large systematic reviews (van Dalen et al. 2011). Only dexrazoxane, a derivate of EDTA, has been approved for cardioprotection in high-risk patients, although benefit and risk of side-effects have to be evaluated from case to case (Lipshultz et al. 2010). General measures like continuous infusion for 48 to 72 hours and use of liposomal DOX are recommended for certain types of cancer, but appear to be insufficient in inhibiting cardiotoxicity (Chung and Youn 2016).

The most effective strategy for preventing heart failure is an early detection of cardiotoxicity and prevention of further progression to irreversible dilative cardiomyopathy

(Chung and Youn 2016). Diagnostic measures ranging from echocardiography to the evaluation of several biomarkers have been discussed with mixed results. Monitoring of cardiac function via strain and strain rate has been shown to be suitable for detection of subclinical changes in LVEF (Thavendiranathan et al. 2014) and cardiac imaging using magnetic resonance imaging (MRI) appears to catch inflammation and edema in early stages (Tamene et al. 2015). However, determined cardiac monitoring in post-chemotherapy care remains to be implemented. While troponins seem promising in predicting cardiac damage (Cardinale et al. 2004), other biomarkers like brain natriuretic peptide show conflicting results (Daugaard et al. 2005). So far, the early detection remains challenging.

Even if ACT is diagnosed early, therapeutic options are limited. Due to lack of studies there are no specific recommendations for the treatment of heart failure following anthracycline treatment (Tan et al. 2015). Therefore, heart failure due to ACT is handled similarly to heart failure of other origins. Treatment with pharmacologic agents including angiotensin-converting enzyme inhibitors, ß-blockers, vasodilators and diuretics is combined with lifestyle modifications. In end-stage heart failure, transplantation surgery is recommended for patients cured of cancer (Yancy et al. 2013).

In order to improve the search for therapeutic and preventive strategies, a distinct understanding of molecular mechanisms causing anti-neoplasticity and cardiotoxicity is needed.

1.1.4 Anti-neoplastic molecular mechanisms

Even after 40 years of routine use in chemotherapy, molecular mechanisms of anthracyclines in cancer cells are still under discussion. Intercalation, alkylation and cross-linking of DNA, inhibition of topoisomerase and free radical formation have been proposed early on (Gewirtz 1999).

DOX is highly concentrated in the nucleus due to a transitioning pathway involving the 26s proteasome. It intercalates in the DNA double-strand and causes cross-links thereby inhibiting replication and transcription in the highly proliferating cells (Minotti et al. 2004).

The enzyme topoisomerase II (TOP2) is located in the nucleus as well and plays a crucial role in replication and transcription by correcting twisted DNA by breaking and resealing the double helix. Binding of DOX to TOP2 leads to an interruption of the process in an intermediate state with cleavaged DNA covalently bound to TOP2 resulting in cell arrest and apoptosis (Binaschi et al. 2001).

Although high levels of reactive oxygen species (ROS) and resulting direct DNA damage was only found for supraclinical DOX concentrations (Gewirtz 1999), production of ROS can damage the cell in numerous ways, which will be further discussed in 1.1.5.1.

1.1.5 Cardiotoxic molecular mechanisms

The underlying mechanisms of ACT are still uncertain and the topic of research today. Lots of studies were performed in animal models and with focus on cardiomyocytes, but insights in human cells and tissue and especially beyond cardiomyocytes are scarce.

So far, the most widely accepted mechanisms include the increase of ROS production, inhibition of TOP2β, the damage of mitochondrial DNA and the impairment of cardiomyocyte function (Figure 1). It appears that ACT manifestation is complex and multifactorial.

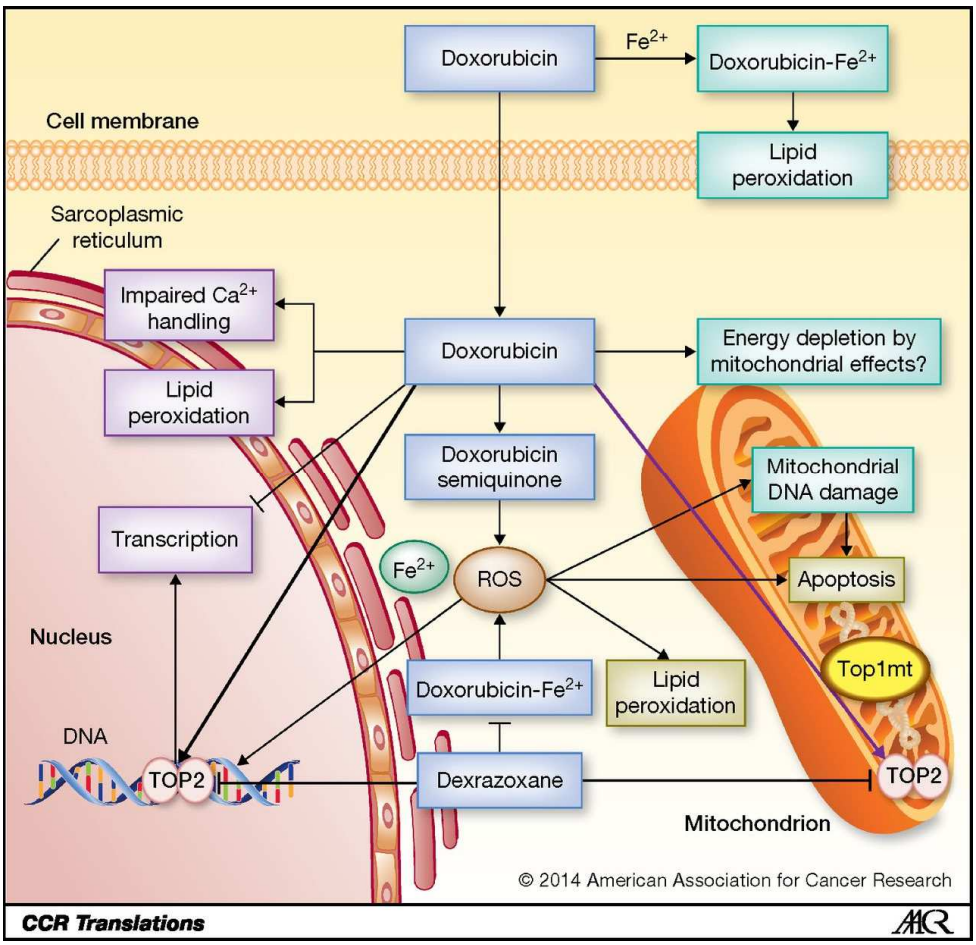

Figure 1: Mechanisms of cardiotoxicity. Doxorubicin damages the cell in multiple ways. The generation of ROS leads to lipid peroxidation, DNA damage and induction of apoptosis. Also, the inhibition of TOP2 causes DNA damage and mitochondrial dysfunction. Lastly, doxorubicin has a negative impact on cardiomyocyte function like Ca^{2+}handling and sarcomeric integrity. From Nitiss and Nitiss (2014), printed with permission of the American Association for Cancer Research.

1.1.5.1 ROS production

The involvement of ROS in the development of ACT has been studied in animal models, cell culture and clinical studies (Doroshow et al. 1980; Nozaki et al. 2004; Ichihara et al. 2007) and is discussed as the main pathomechanism differentiating cardiotoxicity from anti-neoplasticity (Tan et al. 2015).

The oxidative stress theory is further supported as it provides at least a partial explanation for the fact that the heart is damaged while other organs are not. Cardiomyocytes contain large amounts of mitochondria, which are both source and target of DOX-induced ROS (Carvalho et al. 2014). Additionally, cardiomyocytes have a high oxygen consumption but low antioxidant capacity compared to other types of tissue, which are further depleted by DOX treatment (Doroshow et al. 1980; Kaiserová et al. 2007).

Reactive oxygen species is a collective term for different molecules derived from oxygen. The term includes neutral molecules like hydrogen peroxide (H_2O_2), ions like superoxide (O_2-) and radicals like hydroxyl radicals (·OH). The species transition into each other due to their high reactivity. At high concentrations, ROS react with proteins, lipids, carbohydrates, and nucleic acids causing alteration and damage, while at lower concentrations ROS fulfill functions of cell signaling (Brieger et al. 2012).

Two ways of ROS production upon DOX treatment are known. The quinone moiety of anthracyclines can be reduced by electrons from different cellular oxidoreductases to a highly reactive semiquinone, which triggers a further redox cycle in the presence of oxygen ultimately resulting in ROS production (Carvalho et al. 2014) (Figure 2). Because of its redox potential of -320 mV, DOX is favorably reduced by the NADPH-dependent cytochrome P450 reductase, the NADH dehydrogenase of mitochondrial complex I, and nitric oxide synthases (Thornalley and Dodd 1985; Doroshow and Davies 1986; Vásquez-Vivar et al. 1997). Also, anthracyclines can form metal coordination complexes with free metals like iron, triggering a Fenton-type reaction and reduction of oxygen (Demant and Jensen 2005).

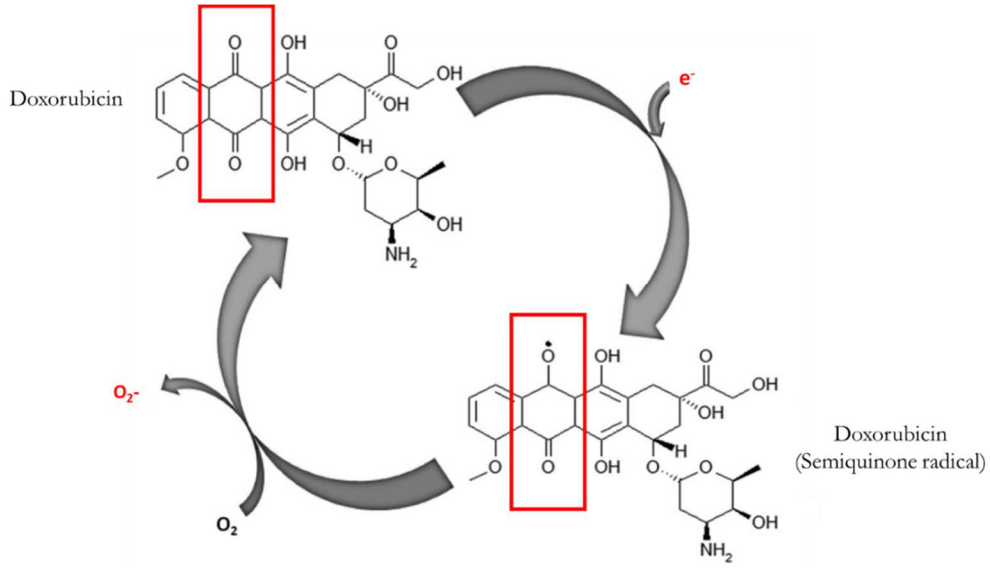

Figure 2: Redox cycling of DOX. Univalent reduction (e-) of the quinone moiety of doxorubicin (top red square) forms a semiquinone radical (bottom red square), which can auto-oxidize via oxygen, generating superoxide anions, reverting to the initial compound. Modified from Carvalho et al. (2014), printed with permission from Wiley-Blackwell.

Oxidative stress damages the cardiomyocytes in multiple ways. ROS cause DNA damage (L'Ecuyer et al. 2006), degradation of the sarcomere (Fu et al. 1990) and mitochondrial dysfunction (Berthiaume and Wallace 2007). Mitochondrial dysfunction may be caused in part by the high affinity of cardiolipin to ROS, a phospholipid in the inner membrane of the mitochondria that is part of energy metabolism (Tokarska-Schlattner et al. 2006).

1.1.5.2 Topoisomerase-II inhibition

Recently, the inhibition of TOP2 has been discussed as a leading cause of ACT. While the isoform TOP2α is lacking in the heart and is overexpressed in cancer cells, the isoform TOP2β is constantly expressed in the heart throughout the cell cycle. Unfortunately, anthracyclines target both isozymes (Wang 2002). The theory is supported by animal studies with TOP2β knockout mice that found a protective effect of TOP2β absence against ACT (Lyu et al. 2007; Zhang et al. 2012). Furthermore, it may explain the inefficacy of other chelators except for dexrazoxane, as dexrazoxane also inhibits binding of anthracyclines to TOP2β (Lyu et al. 2007). Anthracyclines binding to TOP2β has been shown to trigger mitochondrial dysfunction through suppression of the peroxisome proliferator-activated receptor, which regulates oxidative metabolism (Finck and Kelly 2007). This appears to ultimately lead to the activation of p53 and increased apoptosis, β-adrenergic signaling and impaired Ca^{2+}-handling (Tewey et al. 1984).

1.1.5.3 Mitochondrial DNA damage

The mitochondrial DNA encodes a small number of proteins involved in oxidative phosphorylation. On top of mitochondrial dysfunction caused by disruption of energy metabolism at the mitochondrial membrane, both ROS generation and TOP2β inhibition also damage the mitochondrial DNA. As damage to the mitochondria further leads to the generation of ROS and the release of pro-apoptotic molecules this makes mitochondria both target and source of cardiotoxicity caused by anthracyclines (Nitiss and Nitiss 2014). Recently, it was found that knockout mice without mitochondrial topoisomerase I (TOP1mt) were significantly more susceptible to DOX-induced damage as it appeared to increase the reliance on TOP2β (Khiati et al. 2014). Furthermore, alterations to mitochondrial DNA were found in human cardiomyocytes, but not in skeletal muscle, of deceased ACT patients (Lebrecht et al. 2005). This indicates that the cycle of damage to the mitochondrial DNA leading to ROS generation and vice versa may accumulate over time and explains the years of latency leading up to congestive heart failure (Carvalho et al. 2014).

1.1.5.4 Impairment of cardiac function

Ultimately, the multifactorial and complex pathomechanisms of cardiotoxicity lead to the impairment of cardiac function. On the one hand, cardiomyocytes go into apoptosis due to ROS-dependent and -independent mechanisms (Arola et al. 2000). On the other hand, anthracyclines appear to directly impair cardiomyocyte function by disturbing Ca^{2+}homeostasis and damaging structural integrity.

The sarcomeric reticulum is severely disrupted in function via inhibition of the Ca^{2+}-ATPase, direct activation of the ryanodine receptor and an increase in expression of SERCA2a. This leads to electrophysiological disorder and an increase in intracellular Ca^{2+} (Ondrias et al. 1990; Saeki et al. 2002). The excess Ca^{2+} has also been shown to activate calcium-activated proteases called calpains, which leads to the degradation of the sarcomeric protein titin. As a result, elastic properties are lost and myofibrillar disarray occurs (Lim et al. 2004).

As of late, non-cardiomyocyte cells in the heart including cardiac fibroblasts, endothelial cells and cardiac progenitor cells have increasingly been studied in ACT research. It appears that anthracycline treatment has a negative impact on the number of cardiac progenitor cells impairing myocyte turnover (Angelis et al. 2010). Furthermore, fibrosis found in the tissue of end-stage heart failure ACT patients might be caused in part by activation of

cardiac fibroblasts due to chemotherapy (Cappetta et al. 2016). Investigation of non-cardiomyocyte pathophysiology of ACT may give further insights into the complex disease.

1.1.6 Associated gene mutations

Even after considering cumulative dosage and potential risk factors, ACT development still shows high inter-individual variability. It therefore stands to reason that predisposing genetic mutations might explain the variation in ACT incidence. The establishing of associated mutations might open the chance of pretherapeutic risk stratification and could possibly provide further insights into disease pathomechanisms.

A study with 109 ACT patients from the German non-Hodgkin lymphoma study first reported single nucleotide polymorphisms (SNPs) in NADPH oxidase subunits to be significantly associated with ACT manifestation (Wojnowski et al. 2005). Since then, several studies have investigated the role of genetic variants in ACT. A systematic review and meta-analysis from 2017 including 7,092 patients in 28 different studies from 2005 till 2016 found mutations in the genes *CYBA* and *RAC2* to significantly increase the risk of ACT (Leong et al. 2017). An *NCF4* mutation has also been described as a predisposing factor, but results from systematic reviews are conflicting (Reichwagen et al. 2015).

The *cytochrome b-245, alpha polypeptide* (*CYBA*) gene encodes the NADPH oxidase subunit p22phox, an integral component of the functioning enzyme complex for most isoforms. The ACT-associated SNP rs4673 is a missense mutation leading to tyrosine replacing histidine at position 72, which is not affecting the binding between NOX and p22phox in Cos7 or CHO cells (Biberstine-Kinkade et al. 2002). Contradicting functional consequences, both activation in neutrophils (Shimo-Nakanishi et al. 2004) and inactivation in human vascular cells (Guzik et al. 2000) of the SNP have been reported.

The *ras-related C3 botulinum toxin substrate 2* (*RAC2*) gene encodes the protein RAC2, which is needed for assembly and activation of certain NADPH oxidases. The SNP rs13058338 is located in an intron and has been shown to lead to an increase of mRNA expression of RAC2 and NCF4 in whole human blood (Schirmer et al. 2008).

Lastly, the *neutrophil cytosolic factor 4* (*NCF4*) gene encodes the protein p40phox. In its phosphorylated state p40phox acts as an inhibitor of oxidase activity (Lopes et al. 2004). The SNP rs8187710 lies in a putative promoter of the gene. Although direct functional consequences remain to be found, the SNP has been described to be associated with cardiac fibrosis in humans (Cascales et al. 2013).

Even though the study of effects caused by the associated SNPs is unclear and confusing at times, the NADPH oxidase appears to be worth further investigation to deepen the understanding of molecular mechanisms of ACT.

1.1.7 NADPH oxidase

The enzyme containing the associated SNPs described in 1.1.6 is the membrane-bound multi-subunit enzyme complex called nicotinamide adenine dinucleotide phosphate-oxidase or short NADPH oxidase. The fact that the function of NADPH oxidases is the production of ROS further adds to the implication of it being involved in ACT development and predisposition. Of the seven isoforms discovered so far (Brandes et al. 2014), Nox2 and Nox4 are expressed in the heart (Figure 3). Physiological functions include ROS signaling for endothelial cell migration, angiogenesis, vascular tension, smooth muscle growth and inflammatory response (Cave et al. 2006; Zhang et al. 2013), but the mediation of various pathological changes in the heart has been described as well.

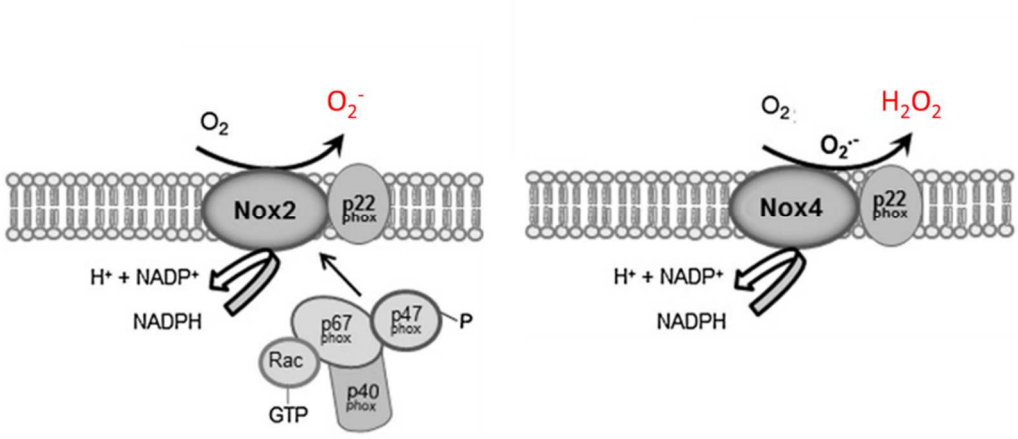

Figure 3: Schematic representation of NADPH oxidase 2 and 4 and their subunits. Catalytic subunits Nox2 and Nox4 are bound to p22hox (*CYBA*) in the membrane. The activation of Nox2 is achieved by the further assembly of the cytosolic complex consisting of p40phox, p47phox, p67phox and Rac2. The electron provided by NADPH is used to create superoxide or hydrogen peroxide. Modified from Zhang et al. (2013), printed with permission from Mary Ann Liebert, Inc.

Nox2 is located at the plasma membrane and produces superoxide. The catalytic subunit of Nox2, also called gp91phox, is bound to and stabilized by the subunit p22phox (Rotrosen et al. 1992). The complex, also called cytochrome b_{558}, remains inactive in the membrane until the assembly of the further subunits p47phox, p67phox, p40phox and Rac2 from the cytosol. The cytosolic subunits activate the membrane complex upon phosphorylation of p47phox via various stimuli (Babior 1999). The involvement of Nox2 in heart failure has

been assessed for several pathomechanisms including ACT characteristic pathologies as cardiomyocyte apoptosis and cardiac fibrosis (Johar et al. 2006; Hayashi et al. 2008; Gilleron et al. 2009). ROS derived from Nox2 has been reported to contribute to ACT via contractile dysfunction, myocardial atrophy, apoptosis and interstitial fibrosis in a mouse model (Zhao et al. 2010) and *in vitro* (Gilleron et al. 2009; Ma et al. 2013).

The location of Nox4 has been discussed to be in the membrane of the endoplasmic reticulum, mitochondria or the nucleus (Lassègue et al. 2012). The catalytic subunit Nox4 is also bound to and stabilized by p22hox, but is constitutively active and regulated through expression in its production of hydrogen peroxide (Martyn et al. 2006). While still up to debate, Nox4 appears to act cardioprotective in heart damage (Zhang et al. 2010).

1.2 Human cardiac fibroblasts

As the cell type responsible for contractility, cardiomyocytes have been the focus of ACT research. However, they make up only 30 to 40 % of the cardiac cell population (Porter and Turner 2009). The most abundant non-cardiomyocyte cells in the heart are cardiac fibroblasts (cFBs) and they are most commonly known for the production and regulation of the extracellular matrix (ECM). With the secretion of collagens, fibronectins and matrix metalloproteinases the cardiomyocytes are embedded in an organized structure, ensuring cardiac functionality (Martin and Blaxall 2012). More and more functions of cFBs and the ECM are discovered implicating a bigger contribution in cardiac homeostasis (Figure 4).

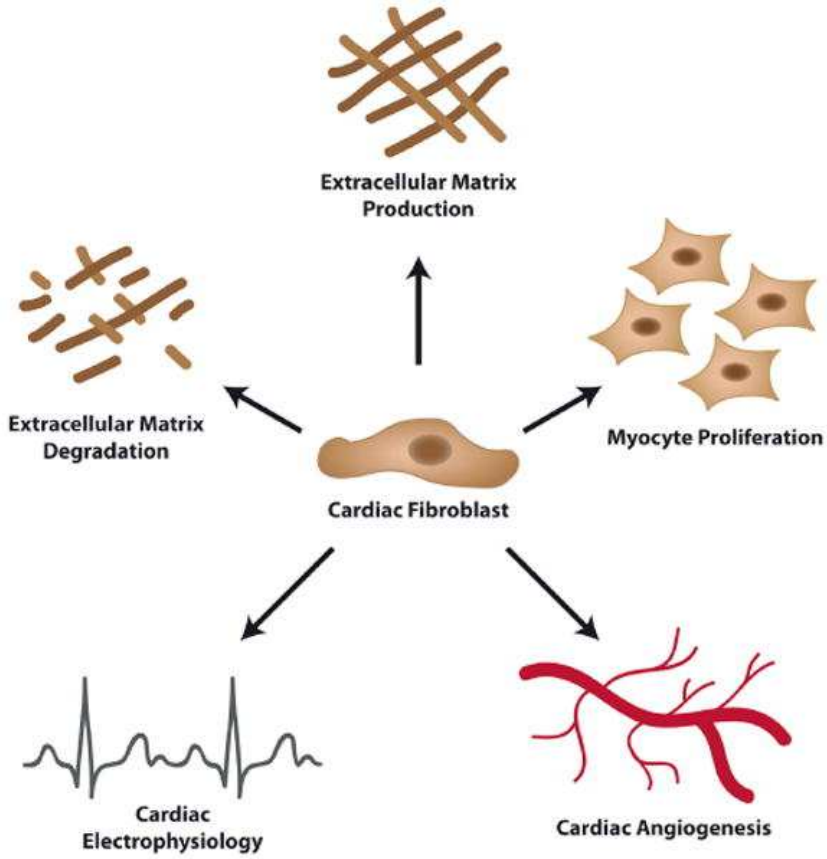

Figure 4: Functions of cardiac fibroblasts. Roles in chemical and mechanical signaling, electrical coupling of cardiomyocytes, contractile force distribution and induction of angiogenesis have been reported. From Krenning et al. (2010), printed with permission from Wiley-Blackwell.

1.2.1 Myofibroblasts and cardiac fibrosis

However, cFBs also contribute to pathologies of the heart. Cardiac injury or stress leads to an excessive proliferation and transdifferentiation of cFBs into myofibroblasts (van Nieuwenhoven and Turner 2013). Pathways of fibroblast activation include several biochemical signaling molecules such as transforming growth factor ß1, angiotensin II, endothelin-1 and platelet-derived growth factor produced by cardiomyocytes, cFBs and inflammatory cells (Leask 2015). Myofibroblasts are differentiated by the expression of contractile proteins and augmented proliferatory and secretory capabilities leading to reparative healing of the myocardium (Deb and Ubil 2014). Chronic myofibroblast activation on the other hand can cause continuing ECM production and fibrotic remodeling (Weber et al. 2013).

An excessive production of ECM leading to cardiac fibrosis contributes to heart failure of various origins including ACT (Unverferth et al. 1983). Cardiac fibrosis can be divided into two forms: reactive fibrosis and replacement fibrosis. While reactive fibrosis affects the

whole heart and is linked to a reduction of myocardial mass, replacement fibrosis is a restoration of dead cardiomyocytes with ECM (Anderson et al. 1979). Either form leads to ventricular stiffening, arrhythmogenicity and myocyte ischemia ultimately causing impairment of diastolic and systolic function (Porter and Turner 2009).

1.2.2 Role in ACT

The contribution of cardiac fibroblasts to ACT manifestation via fibrosis has been reported early on (Unverferth et al. 1983). Recently, novel mechanisms of cFBs in ACT development have been reported. The ataxia telangiectasia mutated (ATM) kinase in cFBs might regulate ACT-related damage through ROS production (Zhan et al. 2016) and loss of the multidrug resistance-associated protein 1 has been shown to potentiate anthracycline damage in cardiac fibroblasts (Zhang et al. 2016). Furthermore, the activation of cFBs to myofibroblasts via transforming growth factor ß1 signaling has been reported to be mediated by the NADPH oxidase 4 (Cucoranu et al. 2005), which in turn might contribute to ACT manifestation, as described in 1.1.7.

Still, the role of cFBs in ACT development is scarcely investigated. Especially a potential involvement in mechanisms of ACT like ROS production and the NADPH oxidase remains to be analyzed.

1.3 Aim of this thesis

The aim of this thesis is to investigate the role of cardiac fibroblasts in the development of ACT in terms of NADPH oxidase subunit expression and ROS production. Fresh left ventricle tissue was obtained from a patient with ACT and a patient with a dilative cardiomyopathy (DCM) of a genetic origin for isolation of cardiac fibroblasts.

Additionally, frozen cardiac tissue from five ACT patients, three DCM patients and three healthy non-failing controls (NF) were to be used to analyze the degree of fibrosis and possible changes in NADPH oxidase subunit expression in chronic heart failure and chronic ACT.

Scientific and technical objectives:

1. Quantification of fibrosis in cardiac tissue of chronic ACT and DCM patients.
2. Isolation of human cardiac fibroblasts from fresh left ventricle tissue.

3. Characterization of the isolated cells for properties and markers typical for cardiac fibroblasts

4. Analysis of the acute reaction of cardiac fibroblasts to anthracycline treatment in terms of NADPH oxidase subunit expression on mRNA and protein level.

5. Analysis of NAPDH oxidase subunit expression in cardiac tissue of chronic ACT and DCM patients on mRNA and protein level.

6. Measurement of anthracycline-induced ROS production in cardiac fibroblasts

Working hypotheses:

1. Human cardiac fibroblasts can be isolated from human cardiac tissue and maintained in culture

2. Cardiac fibroblasts differ from skin fibroblasts in their acute reaction to anthracycline treatment in terms of increased ROS production and change of NADPH oxidase subunit expression.

3. Cardiac fibroblasts from the ACT patient are more sensitive to anthracycline treatment than cardiac fibroblasts from the DCM patient.

4. NADPH oxidase subunit expression varies between ACT patients, DCM patients and healthy controls

2 Materials and methods

2.1 Materials

2.1.1 Cell lines

Human cardiac fibroblasts (CF)

CF ACT 4: Isolated from cardiac tissue of the left ventricle after heart transplantation surgery of a 65-year-old female patient with an anthracycline-induced cardiomyopathy following chemotherapy treatment of a mammary carcinoma, Department of Cardiology and Pneumology, University Medical Center Göttingen

CF DCM 1: Isolated from cardiac tissue of the left ventricle after heart transplantation surgery of a 44-year-old male patient with a genetic dilative cardiomyopathy without chemotherapy in the patient's history, Department of Cardiology and Pneumology, University Medical Center Göttingen

CF healthy: Provided by PromoCell (Heidelberg) #C-12375

CF 3: Isolated from cardiac tissue of the left ventricle of a 19-year-old male patient with a restrictive cardiomyopathy, Department of Cardiology and Pneumology, University Medical Center Göttingen

CF 4: Isolated from cardiac tissue of the left ventricle of a 24-year-old male patient with a genetic dilative cardiomyopathy, Department of Cardiology and Pneumology, University Medical Center Göttingen

CF 5: Isolated from cardiac tissue of the left ventricle, Department of Cardiology and Pneumology, University Medical Center Göttingen

CF 6: Isolated from cardiac tissue of the left ventricle, Department of Cardiology and Pneumology, University Medical Center Göttingen

CF 7: Isolated from cardiac tissue of the left ventricle of a 48-year old male, Department of Cardiology and Pneumology, University Medical Center Göttingen

Human skin fibroblasts (SF)

SF: Isolated from a skin biopsy of the same patient as CF DCM 1

2.1.2 Human cardiac tissue

ACT4: Left ventricle tissue of a 65-year-old female patient with an anthracycline-induced cardiomyopathy following chemotherapy of a mammary carcinoma obtained after heart transplantation surgery, Department of Cardiology and Pneumology, University Medical Center Göttingen

ACT5: University Medical Center Göttingen, tissue bank sample 698. Left ventricle tissue of a 54-year-old male patient with a dilative cardiomyopathy following anthracycline chemotherapy of an Ewing sarcoma

ACT6: University Medical Center Göttingen, tissue bank sample 683. Left ventricle tissue of a 53-year-old female patient with a dilative cardiomyopathy following anthracycline chemotherapy of a Wilms tumor

ACT7: University Medical Center Göttingen, tissue bank sample 693. Left ventricle tissue of a 16-year-old male patient with a dilative cardiomyopathy following anthracycline chemotherapy of a B-cell non-Hodgkin gastric lymphoma

ACT8: University Medical Center Göttingen, tissue bank sample 734. Left ventricle tissue of a 43-year-old male patient with a dilative cardiomyopathy following anthracycline chemotherapy. Tumor unknown.

DCM1: Left ventricle tissue of a 44-year-old male patient with a genetic dilative cardiomyopathy, Department of Cardiology and Pneumology, University Medical Center Göttingen

DCM2: University Medical Center Göttingen, tissue bank sample 723. Left ventricle tissue of a 50-year-old male patient with a dilative cardiomyopathy following a chronic active myocarditis

DCM3: University Medical Center Göttingen, tissue bank sample 719. Left ventricle tissue of a 45-year-old male patient with a dilative cardiomyopathy following an idiopathic eosinophilic myocarditis

DCM4: University Medical Center Göttingen, tissue bank sample 689. Left ventricle tissue of a 52-year-old female patient with a genetic dilative cardiomyopathy

NF1 – 4: Left ventricle non-failing tissue, Department of Cardiology and Pneumology, University Medical Center Göttingen

All procedures were conducted in compliance with the Institutional Ethical Committee, University Medical Center Göttingen, Application: DOK_305_2015. The human samples were achieved in compliance with the local ethical committee (Az. 31/9/00) and written informed consent was received from the participant before inclusion. The study conforms to the World Medical Association declaration of Helsinki.

2.1.3 Media, solutions and factors for cell culture

Table 1: Cell culture material

Name	Supply source
Bovine albumin fraction V solution (BSA, 7.5 %)	Thermo Fisher Scientific #15260037
Dimethyl sulfoxide (DMSO)	Sigma-Aldrich #D2650
DMEM	Thermo Fisher Scientific #11960044
Doxorubicin hydrochloride	Sigma-Aldrich #D1515
DPBS	Thermo Fisher Scientific #14190144
Ethylenediaminetetraacetic acid (EDTA)	Sigma-Aldrich #E6758
Fetal bovine serum (FBS)	Sigma-Aldrich #F7524
L-glutamine (200 mM)	Thermo Fisher Scientific #25030024
Non-essential amino acids (NEAA)	Thermo Fisher Scientific #11140035
Recombinant human basic fibroblast growth factor (hbFGF)	PeproTech #100-18B
ß-Mercaptoethanol (ß-ME)	Serva Electrophoresis #28625
Tris	Roth #5429
Trypsin (1:250)	Thermo Fisher Scientific # 27250018

BSA (0.1 %): BSA (7.5 %) diluted 1:75 with DPBS and stored at 4 °C

ß-ME (100x): 7 µl diluted in 10 ml DPBS, sterile filtrated and stored at 4 °C

hbFGF: 100 mg dissolved in 1 ml of 5 mM Tris and stored at -20 °C. For use in cell culture the stock was diluted 1:10 with 0.1 % BSA for a working concentration of 10 ng/µl and stored at 4 °C

EDTA (50x): 1 g EDTA dissolved in 100 ml DPBS, pH adjusted to 7, sterile filtrated and stored at 4 °C

FBS: heat inactivated at 60 °C for 30 min

Trypsin (0.2 %): 1 g Trypsin dissolved in 1 l DPBS, sterile filtrated and stored at 4 °C

Human fibroblast medium (HFBM): 87 ml DMEM, 10 ml FBS, 1 ml L-glutamine, 1 ml NEAA, 1 ml ß-ME and freshly added hbFGF 1 µg/ml, stored at 4 °C for up to four weeks

0.1 % Trypsin/EDTA (T/E): 50 ml 0.2 % Trypsin, 49 ml DPBS, 1 ml 50x EDTA, stored at 4 °C

Freezing medium: 8 ml HFBM, 2 ml DMSO, hbFGF 2 µg/ml

2.1.4 Disposable articles

Table 2: Disposable material

Name	Supply source
10-cm dish, TC-treated	CytoOne Starlab #CC7682-3394
12-well plate, TC-treated	CytoOne Starlab #CC7682-7512
6-cm dish, TC-treated	CytoOne Starlab #CC7682-3359
6-well plate, TC- treated	CytoOne Starlab #CC7682-7506
96 -well microplate, black	Berthold Technologies #23302
Cell scraper: 2-Posit. Blade 25	Sarstedt #83.1830
Coverslips round 25 mm	R. Langenbrinck #01-0025/2
CryoTube Vials	Thermo Fisher Scientific #377224
Filter tips: 0.1–1000 µL	Starlab #S1120-3810, #S1122-1830, #S1120-1840
Microcentrifuge Polypropylene Tube	Beckman Coulter #357448
Multiplate 96-Well PCR Plate, clear	Bio-Rad #mll9601
Object slides (76 x 26 mm)	Thermo Fisher Scientific #10143562C
PCR Plate Heat Seal	Bio-Rad #1814030
Pipettes: 5 mL, 10 mL, 25 mL	Sarstedt #86.1253.001, #86.1254.001, #86.1685.001

Name	Supply source
Polypropylene Screw Neck Vial, with Cap and PTFE/silicone Septum	Waters #186002640
Stericup-HV (0.45 µm)	Merck Millipore #SCHVU05RE
Steriflip-GP (0.22 µm)	Merck Millipore #SCGP00525

2.1.5 Commercial kits

Table 3: Commercial kits

Name	Supply source
Amplex Red Hydrogen Peroxide/Peroxidase Assay Kit	Thermo Fisher Scientific #A22188
Immobilon Western Chemiluminescent HPR Substrate	Milipore #WBKLS0500
Maxwell 16 cell DNA purification kit	Promega #AS1020
Pierce Coomassie Plus (Bradford) Assay Kit	Thermo Fisher Scientific #23236
QIAquick gel extraction kit	Qiagen #28706
ReliaPrep RNA Tissue Miniprep System	Promega #Z6110
SV total RNA isolation system	Promega #Z3105
Trans-Blot Turbo RTA Mini Nitrocellulose Transfer Kit	Bio-Rad #1704270

2.1.6 Buffers, solutions and chemicals for molecular biological analysis

Table 4: Molecular biology material

Name	Supply source
4', 6-Diamidino-2-phenylindole dihydrochloride (DAPI)	Sigma-Aldrich #D9542
Ammonium persulfate (APS)	Roth #9178
Boric acid	Sigma-Aldrich #15663
cOmplete (protease inhibitor cocktail tablets)	Roche #04693132001
Dithiothreitol (DTT)	Roth #6908
dNTP mix	Bioline #BIO-39029
Fluoromount-G	eBioscience #00-4958-02
Gelatin	Sigma-Aldrich #48720
GeneAmp 10X PCR Puffer II & $MgCl_2$	Thermo Fisher Scientific #4379878
GeneRuler 100 bp Plus DNA Ladder	Thermo Fisher Scientific #0321
Glycine	Roth #3908
GoTaq G2 DNA polymerase	Promega #M7845
Hydrochloric acid fuming 37 % (HCl)	Merck Millipore #100317
IGEPAL CA-630	Sigma-Aldrich #I3021
Isopropanol	Merck Millipore #109634
Laemmli Sample Buffer (4x)	Bio-Rad #161-0747
Magnesium chloride ($MgCl_2$)	Sigma-Aldrich #M8266
Methanol	Merck Millipore #106009

Name	Supply source
Midori Green Advance	Biozym #617004
MuLV reverse transcriptase (50 U/µl)	Thermo Fisher Scientific #N808-0018
Non-fat dry milk	Roth #T145
Nuclease-free water	Thermo Fisher Scientific #AM9932
Oligo d(T)16 (50 µM)	Thermo Fisher Scientific #N808-0128
Paraformaldehyde (PFA)	Sigma-Aldrich #158127
peqGold universal agarose	Peqlab #35-1020
PhosStop (phosphatase inhibitor cocktail tablets)	Roche #04906837001
Ponceau S solution	Sigma-Aldrich # P7170-1L
Potassium chloride (KCl)	Sigma-Aldrich #P9541
RNase inhibitor (20 U/µl)	Thermo Fisher Scientific #N808-0119
Rotiphorese gel 30	Roth #3029
Sodium chloride (NaCl)	Roth #9265.1
Sodium dodecyl sulfate (SDS)	Roth #2326
Sodium fluoride (NaF)	Roth #P756
Sodium orthovanadate (Na_3VO_4)	Sigma-Aldrich #S6508
SYBR Green PCR Master Mix	Thermo Fischer Scientific #4309155
Tetramethylethylenediamine (TEMED)	Roth #2367
Triton X-100	Sigma-Aldrich #3051.3
Tween 20	Bio-Rad #170-6531

TB-Buffer (5x): 54 g Tris, 27.5 g boric acid, filled up to 1 l with dH_2O

Agarose gel (1.5 %): 1.5 g Agarose dissolved in 100 ml 1x TB-Buffer, after boiling in microwave 0.07 µl/ml Midori Green was added for visualization under UV-light

DAPI: Stock solution: 2 mg DAPI dissolved in 1 ml dH_2O, stored at 4 °C. Diluted 1:500 in 1 % BSA for working solution

PFA (4 %): 4 g PFA dissolved in 100 ml DPBS, stored at -20 °C

Triton X-100 (0.1 %): 1 µl Triton X-100 diluted in 999 µl DPBS

Tris-HCl pH 7.4 (2 M): 12.114 g Tris dissolved in 100 ml dH_2O, pH adjusted to 7.4 with HCl

Cell lysis buffer: 100 µl 2M Tris-HCl pH 7.4, 500 µl 4M NaCl, 1 ml 200 mM NaF, 1 ml 10 % Igepal, 100 µl 100 mM Na_3VO_4, 100 µl 1 mM DTT, 1 tablet of PhosStop, 1 tablet of cOmplete, 5.2 ml dH_2O, always prepared fresh under exclusion of light

TBS-Buffer (10x): 24.2 g Tris, 29.24 g NaCl, filled up to 1 l with dH_2O

TBST-Buffer (1x): 100 ml 1x TBS-Buffer, 900 ml dH_2O, 1 ml Tween 20

Tris-HCl/SDS, pH 6.8: 6.05 g Tris and 0.4 g SDS dissolved in 100 ml dH_2O, pH adjusted to 6.8 with HCl

Tris-HCl/SDS, pH 8.8: 18.2 g Tris and 0.4 g SDS dissolved in 100 ml dH_2O; pH adjusted to 8.8 with HCl

APS (10 %): 10 g APS dissolved in 100 ml H_2O, stored at -20 °C

10% separating gel: 4 ml Acrylamide, 3 ml Tris-HCl/SDS pH 8.8, 5 ml H_2O, 48 µl 10 % APS, 18 µl TEMED, gently mixed and immediately poured

Stacking gel: 1 ml Acrylamide, 1.88 ml Tris-HCl/SDS pH 6.8, 4.62 ml H_2O, 37.5 µl 10% APS, 15 µl TEMED

Running buffer: 3 g Tris, 14.4 g Glycine and 1 g SDS, filled up to 1 l with dH_2O

Milk (5 %): 5 g non-fat dry milk dissolved in 100 ml dH_2O

2.1.7 Buffers, solutions and chemicals for analysis of reactive oxygen species

Table 5: ROS analysis material

Name	Supply source
Acetonitrile (HPLC-grade)	Merck # 100017
Amplex Red reagent	Thermo Fisher Scientific # A12222
Dihydroethidium (DHE)	Sigma-Aldrich #D7008
Horseradish peroxidase (HRP)	Thermo Fisher Scientific # 31491B
Nicotinamide adenine dinucleotide phosphate (NADPH)	Sigma-Aldrich #N5130
Superoxide dismutase (SOD)	Sigma-Aldrich #S9697
Trifluoroacetic acid	Merck # 113363

Lysis buffer for membrane fractions: 605 mg Tris, 3 mg EDTA, fill up to 100 ml with dH_2O and adjust pH to 7.4 with HCl

Amplex Red working solution 1: 1.6 µl 10 mM Amplex Red, 3.2 µl 10 U/ml HRP, 315.2 µl 1x reaction buffer, always prepared fresh under exclusion of light

Amplex Red working solution 2: 6.5 µl 10 mM Amplex Red, 13 µl 10 U/ml HRP, 630.5 µl 1x reaction buffer, always prepared fresh under exclusion of light

2.1.8 Oligonucleotides

Oligonucleotides for polymerase chain reaction (PCR) were purchased from Microsynth AG, Switzerland. Genes are listed in alphabetical order with sequence, length of amplified fragment in base pairs (F) and annealing temperature in °C (T) in **Table 6**

Table 6: Oligonucleotides used for PCR

Gene	Sequence	F	T
NCF4	For: 5'- ACAGGAAAATGGAGGCCAGC -3' Rev: 5'- ATTGAGGAAGTGGACCCTCG -3'	252	60
RAC2	For: 5'- TTGCCCTGAGAACCAAGACC -3' Rev: 5'- CGCTGCTATTTCATGGCTGG -3'	299	60
CYBA	For: 5'- CAACCCTTTGGTGCTTGTGG -3' Rev: 5'- CAAGCCCTCCTGAGCCCTA -3'	288	60

Oligonucleotides for quantitive real-time polymerase chain reaction (qRT-PCR) were purchased from Microsynth AG, Switzerland. Genes are listed in alphabetical order with sequence and length of the amplified fragment in base pairs (F) in **Table 7**

Table 7: Oligonucleotides used for qRT-PCR

Gene	Sequence	F
COL1A1	For: 5'-AGACAGTGATTGAATACAAAACCA-3' Rev: 5'-GGAGTTTACAGGAAGCAGACA -3'	130
CTGF	For: 5'- TTGGCAGGCTGATTTCTAGG -3' Rev: 5'- GGTGCAAACATGTAACTTTTGG -3'	193
CYBA	For: 5'- CAACCCTTTGGTGCTTGTGG -3' Rev: 5'- CAAGCCCTCCTGAGCCCTA -3'	288
FSP1	For: 5'-TCTTTCTTGGTTTGATCCTGACT-3' Rev: 5'-AGTTCTGACTTGTTGAGCTTGA-3'	130
GAPDH	For: 5'- AGAGGCAGGGATGATGTTCT -3' Rev: 5'- TCTGCTGATGCCCCCATGTT -3'	258
NCF1	For: 5'- GTCCTGACGAGACGGAAGAC -3' Rev: 5'- TGACGTCGTCTTTCCTGATGA -3'	171
NCF2	For: 5'- CAGAAAGTGAACACCTTGGGG -3' Rev: 5'- GCCAAATCATATTTCTCTGTCTGGT -3'	382
NCF4	For: 5'- CCTCCTCAGTCGGATCAACAA -3' Rev: 5'- CTCCCAGGCCACAGACTTGAT -3'	181

Gene	Sequence	F
NOX2	For: 5'- GCAGCCTGCCTGAATTTCA -3' Rev: 5'- TGAGCAGCACGCACTGGA -3'	93
NOX4	For: 5'- GCAGGAGAACCAGGAGATTG -3' Rev: 5'- CACTGAGAAGTTGAGGGCATT -3'	125
P22PHOX	For: 5'- GTACTTTGGTGCCTACTCCA -3' Rev: 5'- CGGCCCGAACATAGTAATTC -3'	167
POSTN	For: 5'- ACAAGAAGAGGTCACCAAGGTC -3' Rev: 5'- CTTCCTCACGGGTGTGTCTC -3'	109
RAC1	For: 5'- ATG CAC CGC TAC GAC GTG A -3' Rev: 5'- CTT TTG CAC CCC TCC CAT TT -3'	199
RAC2	For: 5'- AAGAAGCTGGCTCCCATCACCTAC -3' Rev: 5'- AACACGGTTTTCAGGCCTCTCTG -3'	113
TCF21	For: 5'- CAACCTGACGTGGCCCTTTA -3' Rev: 5'- TGGTTCCACATAAGCGGCTC -3'	86
α-SMA	For: 5'-AAGCACAGAGCAAAAGAGGAAT -3' Rev: 5'-ATGTCGTCCCAGTTGGTGAT -3'	76

2.1.9 Antibodies

Table 8: Primary antibodies

Antigen	Host, Isotype	Dilution		Supply source
		WB	**IF**	
COL1	Rabbit, IgG	-	1:3000	Abcam #ab34710
GAPDH	Mouse, IgG	1:500		Merck #MAB374
NOX2	Mouse, IgG	1:2000		BD Transduction Laboratories #611414
NOX4	Rabbit, IgG	1:2000		Abcam #ab109225
RAC2	Mouse, IgG	1:1000		Sigma-Aldrich #SAB1404292
SERCA	Mouse, IgG	1:10000		Thermo Fisher Scientific #MA3-919
α-SMA	Mouse, IgG	-	1:50	Sigma-Aldrich #A-2547

Table 9: Secondary antibodies

Antigen	Conjugate	Host	Dilution	Supply source
Mouse IgG	AlexaFluor 488	Donkey	1:1000	Thermo Fisher Scientific #A-21202
Rabbit IgG	AlexaFluor 647	Goat	1:500	Thermo Fisher Scientific #A-31573
Mouse IgG	HRP	Sheep	1:10000	GE Healthcare #NA9310-1ML
Rabbit IgG	HRP	Donkey	1:10000	GE Healthcare #NA9340-1ML

2.1.10 Hardware

Table 10: Hardware

Name	Supply source
Accu-jet pro	Brand
Balances: Extend ED153-CW, CPA225D	Sartorius
BioPhotometer	Eppendorf
Centrifuges: 5810R, 5415D, 5415R	Eppendorf
Cryo-Safe -1 °C freeze controller	Bel Art
DNA Maxwell 16 System	Promega
HERACELL VIOS 160i CO2 Incubator	Thermo Fisher Scientific
HPLC system with rheodyne injector, photodiode array detector (W2996) and fluorescence detector (W2475)	Waters
iCycler Thermal Cycler, iQ5 Multicolor Real-Time PCR Detection System	Bio-Rad
inoLab pH 7110	WTW
MICCRA D-9 Homogenizer	Miccra
Microscopes: Axio Oberserver A1, Axio Oberserver Carl Z1, Primo Vert, Axiovert 25	Zeiss

Name	Supply source
Milli-Q Reference Water preparation system	Merck Millipore
Mini-PROTEAN Tetra Vertical Electrophoresis Cell	Bio-Rad
Mithras² LB 943	Berthold Technologies
Molecular Imager ChemiDoc XRS+	Bio-Rad
Neubauer improved counting chamber	Marienfeld Superior
Nova-Pak C_{18} column	Waters
Pipettes: Reference, Research plus (10/100/1000 µL)	Eppendorf
Power Pac 3000-Power supply	Bio-Rad
Sterile bench: Laminar air flow cabinet	Heraeus Instruments
Thermocycler 48	SensoQuest
TL 100 Ultracentrifuge	Beckmann
Trans-Blot Turbo Transfer System	Bio-Rad

2.1.11 Software

Table 11: Software

Name	Supply source
AxioVision	Carl Zeiss
ApE	M. Wayne Davids
Chromeleon 6.8 chromatography data system	Dionex
Image Lab 6	Bio-Rad
IQ optical system software	Bio-Rad
Mikrowin 2000/2010	Mikrotek Laborsysteme GmbH

Name	Supply source
OlyVia	Olympus
Prism 6/7	GraphPad Software, Inc

2.2 Methods

2.2.1 Cell culture

All cells were cultured under humidified conditions of 5 % CO_2 and 20 % H_2O at 37 °C. Cell culture work was done under sterile conditions in a laminar air flow sterile bench.

2.2.1.1 Isolation and cultivation of human cardiac fibroblasts and skin fibroblasts

Fresh human cardiac tissue from the left ventricle myocardium and tissue from the dermis section of a skin biopsy, each with a size of approximately 1 mm^3 was plated on 6 cm cell culture dishes in human fibroblast medium (HFBM). To secure attachment and proliferation of the fibroblasts, the dish was left without medium change for one week, after which the tissue was removed.

The obtained primary human cardiac and skin fibroblasts were continuously cultured in HFBM. Medium was changed every to every second day and the cells were passaged every 3 - 6 days, depending on individual growth rate and passage. To achieve detachment, the cells were washed once with 0.1 % T/E and directly afterwards treated with 0.1 % T/E for 30 - 60 seconds, depending on the cell line. The cells were then removed from the dish with HFBM and replated in appropriate dilution.

2.2.1.2 Freezing of human fibroblasts

To store the cells for long periods of time, they were frozen in liquid nitrogen. Two to four days after passage at around 85 % confluency the cells were detached as described in 2.2.1.1, transferred into a 15 ml tube containing HFBM and centrifugated at 1000 rpm for 5 min. The pellet was then resuspended in 1 ml freezing medium and transferred into a cryotube vial, which was placed in a Cryo-Safe -1 °C freeze controller. The box was frozen for 24 hours at -80 °C. Afterwards the vials were finally stored in liquid nitrogen.

2.2.1.3 Thawing of human fibroblasts

Recultivation of frozen cells was achieved by thawing the cryotube vial in a 37 °C water bath until only few ice crystals were still visible. The cell suspension was then transferred into a 15 ml tube containing 10 ml of cold HFBM, gently mixed and centrifuged at 1000 rpm for 5 min. The pellet was resuspended in 1 ml HFBM and plated on appropriately sized cell culture dish.

2.2.1.4 Preparation of cell samples for analysis

To preserve cell samples for later analysis, pellets were prepared and frozen. First, after possible treatments, the cells were washed 3 times with DPBS and suspended in 1 ml DPBS using a cell scraper. The suspension was then transferred to a 1.5 ml vial and centrifuged at 10000 rpm for 2 min. The supernatant was carefully removed and the remaining pellet snap-frozen in liquid nitrogen for a few minutes. Finally, the sample was stored at -80 °C.

2.2.2 DNA isolation and sequencing

To identify single nucleotide polymorphisms (SNPs) in the human cardiac tissue and in human fibroblasts, genomic DNA needed to be isolated from the tissue or cells. The Maxwell 16 DNA Purification Kit (Promega) was used with a Maxwell 16 instrument as described in the manufacturer's protocol. Afterwards the DNA concentration was measured with a BioPhotometer at 260 nm.

Next, a template containing the SNP site was amplified by PCR, as described in 2.2.3.4. The band with the expected size was then cut out and the DNA purified using the QIAquick gel extraction kit (Qiagen), as described in the manufacturer's protocol.

Finally, the sequencing was performed by Seqlab Sequencing Laboratories GmbH, Göttingen, and the generated chromatograms analyzed with ApE.

2.2.3 Gene expression analysis

For exploration of mRNA expression in the human fibroblasts and human cardiac tissue mRNA was first isolated from the cells, reverse transcribed into cDNA and finally analyzed by quantitive real-time PCR.

2.2.3.1 mRNA isolation from human fibroblasts

Either frozen pellets or fresh cells after 3 washing steps with DPBS were suspended in 200 – 500 µl RNA lysis buffer. Total RNA was then purified using the SV total RNA isolation system (Promega), as stated by the manufacturer's protocol. Next, RNA concentration and purity were measured with a BioPhotometer at 260 nm and 280 nm. Finally, the RNA samples were used for further analysis or frozen at -80 °C.

2.2.3.2 mRNA isolation from human cardiac tissue

First, an approximately 4mm³ big and approximately 8 - 15 mg heavy piece of tissue was cut off with a scalpel in a bath of liquid nitrogen filled into a bowl prepared of aluminum beforehand to avoid thawing. The piece was then transferred into a 1.5 ml reaction tube containing 500 µl of RNA lysis buffer and homogenized using the MICCRA D9-Homogenizer. Three steps of homogenization were performed, each for 8 seconds and with cooling on ice for 1 min in between. The RNA was subsequently purified using the

ReliaPrep RNA Tissue Miniprep System (Promega), as stated by the manufacturer's protocol and eluted in a volume varying between 15 µl and 30 µl. Next, RNA concentration and purity were measured with a BioPhotometer at 260 nm and 280 nm. Finally, the RNA samples were used for further analysis or frozen at -80 °C.

2.2.3.3 Reverse transcription into cDNA

In order to analyze mRNA expression, the RNA needed to be reverse transcribed into complementary DNA (cDNA) first. The components for a single reverse transcription (RT) were prepared as the following reaction mix:

100 ngRNA + Nuclease-free H_2O	10.2 µl
10x PCR buffer II	2 µl
25 mM $MgCl_2$	4 µl
100 mM dNTPs	0.8 µl
RNase Inhibitor (20 U/µl)	1 µl
50 µM Oligo (dt)16	1 µl
MuLV Reverse Transcriptase (50 U/µl)	1 µl
Final volume	20 µl

The RT reaction was performed in a thermal cycler (SensoQuest) running the following program:

10 min	22 °C
50 min	42 °C
10 min	95 °C

2.2.3.4 Polymerase chain reaction (PCR)

To amplify certain cDNA templates of interest by PCR, the following reaction mix was prepared with the suitable primers:

cDNA	2 µl
5x Green GoTaq Reaction Buffer I	5 µl
10 mM dNTPs	1.6 µl
Primer forward (10 pmol/µl)	1 µl
Primer reverse (10 pmol/µl)	1 µl
GoTaq DNA Polymerase	0.1 µl
Nuclease-free H_2O	14.3 µl
Final volume	25 µl

The PCR was performed in a thermal cycler (SensoQuest) running the following program:

2 min	95 °C	
15 sec	95 °C	35 repeats
15 sec	60 °C	
30 sec	72 °C	
10 min	72 °C	

To detect the amplified product, the DNA fragments were separated via agarose gel electrophoresis at 100 V for 45 min and visualized under UV-light.

2.2.3.5 Quantitive Real-Time PCR (qRT-PCR)

Quantification of mRNA expression was achieved by amplification of the cDNA template of interest and measuring fluorescence of the DNA-intercalating agent SYBR Green. The fluorescence signal in the sample was compared to a standard curve of known concentrations of the template and calculated to the starting quantity by the iQ5 software.

First, the standard curve was prepared by performing a polymerase chain reaction as described in 2.2.3.5 with primers enveloping the gene of interest and purification of the product as described in 2.2.2. After measuring cDNA concentration, a serial dilution with standards ranging from 1 ng/µl to 1.25 fg/µl was prepared and frozen at -20 °C.

For the measurement a reaction mix as described below was prepared for each well:

cDNA	1 µl
SYBR Green Mix	10 µl
Primer forward (10 pmol/µl)	1 µl
Primer reverse (10 pmol/µl)	1 µl
Nuclease-free H2O	7 µl
Final volume	20 µl

For each sample and standard duplicates were measured as the cDNA was amplified using the following program:

2 min	95 °C	
15 sec	95 °C	40 repeats
10 sec	60 °C	
20 sec	72 °C	
10 min	95 °C	
10 sec	95 °C – 60 °C	[melting curve]

2.2.4 Western blot analysis

To investigate protein expression in the human fibroblasts and the human cardiac tissue, total protein was isolated, separated by SDS-polyacrylamide electrophoresis, transferred to a nitrocellulose membrane and incubated with HRP-conjugated antibodies.

2.2.4.1 Protein isolation

The frozen cell samples were resuspended in 50–100 µl of cell lysis buffer, depending on pellet size. The human tissue was homogenized in 250 µl cell lysis buffer as described in 2.2.3.2. After 30 min incubation on ice, the samples were centrifuged at 4 °C at 3000 rpm for 8 min. The supernatant containing the total protein was then transferred to a new 1.5 ml tube. Protein concentration was measured using the Coomassie Plus (Bradford) Assay Kit (Thermo Fisher Scientific), as described in the manufacturer's protocol. Lastly, a mix containing 1 µg/µl of protein was prepared with Laemmli-buffer (see 2.1.6) and cell lysis buffer for electrophoresis and denaturated at 90 °C for 5 min. The samples were then frozen at -20 °C or used directly for further analysis.

2.2.4.2 SDS-polyacrylamide electrophoresis

Protein separation was achieved by loading 15 µl of the samples (15 µg) and 6 µl of protein ladder in separate wells in a gel consisting of stacking gel and 10 % separating gel, placed in a tank filled with running buffer. The electrophoresis was carried out at 15 mA per gel for 90–120 min.

2.2.4.3 Transfer and imaging

The blotting of the separated protein onto the membrane was carried out using the Trans-Blot Turbo RTA Mini Nitrocellulose Transfer Kit (Bio-Rad), as described in the manufacturer's protocol. The membrane was subsequently stained with Ponceau red solution and washed with dH_2O as a control of the successful transfer. Next, the membrane was blocked with 5 % milk for one hour, after which the first antibody in 1 % milk was incubated overnight at 4 °C. After three washing steps with TBST, 10 min each, the second antibody in 1 % milk was incubated for one hour at room temperature and washed away with TBST three times, 10 min each. Lastly, the protein-bound antibodies were visualized using the Immobilon western chemiluminescent HRP substrate (Millipore) in a Molecular Imager ChemiDoc XRS+ (Bio-Rad).

2.2.5 Immunocytochemistry

To visualize certain proteins on a cellular level, immunofluorescence analysis was performed. The cells were plated on round glass coverslips in a cell culture dish and cultured for a day. After washing the cells three times with DPBS, fixation was performed by a 20 minute incubation with 4 % PFA. Afterwards the cells were blocked in 1 % BSA for at least 24 hours at 4 °C.

The staining was performed with Triton X-100 added to the antibodies. After three washing steps with DPBS, the first antibody was added and incubated overnight at 4 °C. After another three washing steps with DPBS, the second antibody was added and incubated for one hour at room temperature. After another three washing steps with DPBS, the cells were stained with DAPI for 10 min at room temperature. Finally, the cells were washed again three times with DPBS and once with dH_2O and subsequently mounted with Fluoromont-G on object slides and sealed with nail polish.
The slides were stored at 4 °C in the dark and analyzed with a Zeiss AxioCam MRm 1.4MP camera.

2.2.6 Amplex Red assay

Extracellular hydrogen peroxide (H_2O_2) production of the human fibroblasts was assessed with the Amplex Red Hydrogen Peroxide/Peroxidase Assay Kit (Invitrogen), as described in the manufacturer's protocol. The change of colorless Amplex Red to fluorescent resorufin in the presence of HRP and H_2O_2 was measured with a Mithras^2 LB 943 platereader. An H_2O_2 standard curve was used to calculate extracellular H_2O_2 in the samples.

2.2.7 Preparation of membrane fractions

The human fibroblasts were plated on a 10-cm cell culture dish and cultivated to a confluence of around 85 % and a cell number of 1.5 – 3 million cells. After potential treatments, the cells were washed twice with cold DPBS and harvested in 500 µl of lysis buffer for membrane fractions with a cell scraper. Next, the sample was sonicated three times for 10 seconds each at 8 W. To separate intact cells, nuclei and mitochondria, the sample was centrifuged at 18000 rpm for 15 min. The supernatant was further centrifuged at 47000 rpm for 1 hour at 4 °C, which led to a pellet of membrane-enriched fraction that was frozen away at -80 °C and used for further experiments.

2.2.8 DHE-HPLC

To analyze superoxide production in the membrane fraction of the human fibroblasts, the turnover of dihydroethidium (DHE) to 2-hydroxyethidium (2-EOH) was measured by high-performance liquid chromatography (HPLC). DHE has been shown to react upon oxidation from different forms and sources of ROS into different compounds. When oxidized by superoxide, 2-EOH is formed, while the reaction with hydrogen peroxide and metal-based oxidizing systems leads to the formation of ethidium (Zhao et al. 2003; Fink et al. 2004). The compounds can then be measured by HPLC and the ratio of 2-EOH divided by DHE can be used to estimate the production of superoxide (Laurindo et al. 2008).

Ten µg of the membrane fraction protein were incubated with 100 µM DHE for 30 min in the dark. Additionally, for each sample, three conditions were prepared and incubated

together with the DHE: 1) with 300 μM NAPDH, 2) without the NADPH, and 3) with 500 U/ml SOD and 300 μM NAPDH. The reaction was then stopped on ice until HPLC injection, which was done over a period of 6 – 10 hours. Chromatographic separation was achieved in a gradient condition of acetonitrile and dH_2O in a reversed-phase C_{18} column. The separated 2-EOH and DHE were measured by fluorescence detection at 510/595 nm.

2.2.9 Quantification of fibrosis in human cardiac tissue

The frozen cardiac tissue of ACT and DCM patients, as well as healthy controls was embedded and sliced by technician Sandra Berès-Georgie and stained with Masson's trichrome staining in cooperation with the Department of Pathology of the University Medical Center Göttingen (Dr. Hanibal Bohnenberger). Next, the area of fibrosis was quantified in cooperation with the Department of Clinical Optical Microscopy (Gertrude Bunt, Andre Sasse). First the slides were scanned for virtual microscopy using a 20x objective (UPlanApo) with the dotSlide SL slide scanner (Olympus) and a peltier-cooled XC10 camera. Lastly, fibrotic areas were calculated by using the cellSens Dimensions software (Olympus).

2.2.10 Statistical analysis

In the following work, data is depicted as mean ± standard error of mean (SEM). For data sets consisting of two groups, the two-tailed Student's t-test was used. For data sets with more than two groups, one-way or two-way analysis of variance (ANOVA) was applied. Statistical significance is depicted as *=$p<0.05$, **=$p<0.01$, ***=$p<0.001$, ****=$p<0.0001$. Statistical analysis was done with Prism 7 (GraphPad).

3 Results

3.1 Quantification of fibrosis in human cardiac tissue

To establish the importance of cardiac fibroblasts in the development and manifestation of anthracycline-induced cardiotoxicity and provide a segue into the work done in this study, human explant cardiac tissue of ACT patients and DCM patients of varying pathomechanisms, as well as healthy controls were quantified for fibrotic areas in relation to myocardium.

Firstly, the tissue was stained with Masson's trichrome staining in which collagen is stained in blue, while muscle tissue is stained in red (Figure 5).

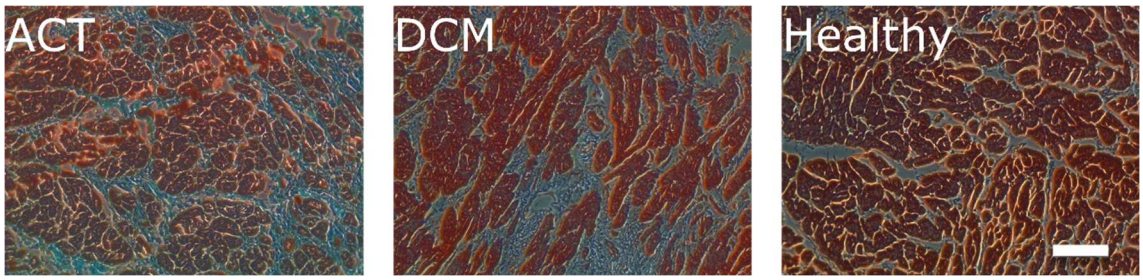

Figure 5: Typical stainings of human cardiac tissue. Cardiac tissue from the ACT-4 patient (ACT), cardiac tissue from the DCM-3 patient (DCM) and healthy cardiac tissue (Healthy) after trichrome staining under light microscopy in 10x magnification. Scale bar: 100 μm

The stainings were subsequently analyzed for fibrotic areas and quantified in relation to myocardium.

Fibrosis was significantly higher in ACT and DCM patients compared to healthy controls with a mean of 24.2 % fibrosis in ACT tissue, 23 % fibrosis in DCM tissue and 8.5 % fibrosis in healthy tissue (Figure 6).

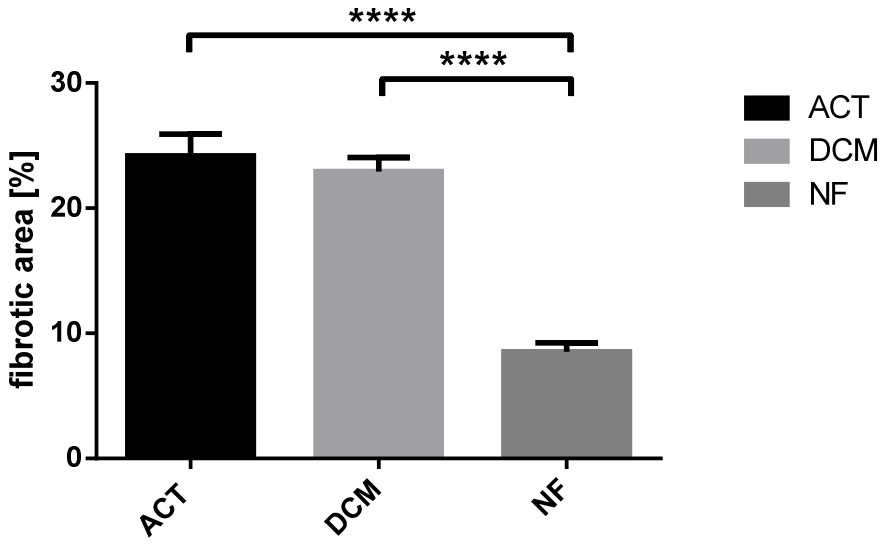

Figure 6: Percentage of fibrotic areas in human cardiac tissue. Quantification of trichrome stainings of cardiac tissue from ACT patients (ACT, n=5 patients (biological replicates)), cardiac tissue from DCM patients (DCM, n=5) and healthy non-failing cardiac tissue (NF, n=4) showing increased fibrosis in the patient groups. Three technical replicates for each biological replicate.

In conclusion, ACT and DCM patients show significantly larger fibrotic areas compared to healthy control tissue.

3.2 Characterization of human cardiac fibroblasts

Human cardiac fibroblasts were obtained by plating fresh human cardiac tissue from the left ventricle muscle on a cell culture dish in human fibroblast medium. Attaching and proliferating cells were assumed to be human cardiac fibroblasts. As this method of isolation is not yet established to be highly specific for the proclaimed cell type, further characterization of the cells was warranted. This included morphology comparison, quantification of cell growth, analysis of gene expression and immunostaining. The isolated cells were from the ACT-4 patient (CF ACT) and the DCM-1 patient with a genetic background (CF DCM). As a positive control, healthy human cardiac fibroblasts obtained from PromoCell (CF Healthy) were used. Furthermore, skin fibroblasts from the DCM-1 patient (SF), isolated from the dermis of a skin biopsy, were used as a negative control to discriminate the different types of fibroblasts.

3.2.1 Morphology comparison

The first step to characterize the presumable human cardiac fibroblasts was to compare their celluluar morphology under light microscopy. All four cell lines showed fibroblast characteristics such as large, roughly triangular cell bodies, large nuclei and irregular cell protrusions connecting the cells (Figure 7).

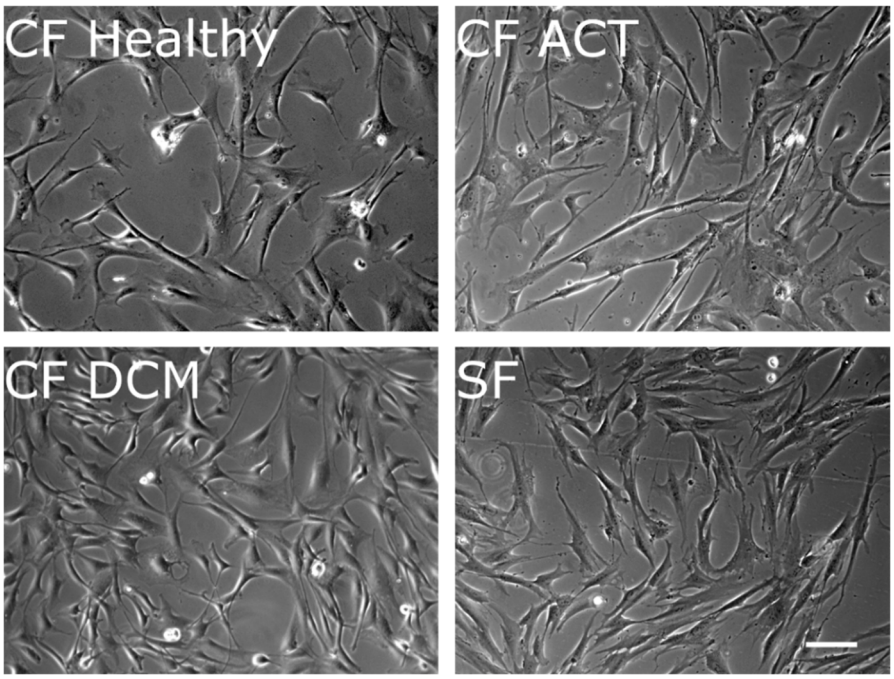

Figure 7: Morphology of human fibroblasts. Healthy cardiac fibroblasts (CF Healthy), cardiac fibroblasts from the ACT-4 patient (CF ACT), cardiac fibroblasts from the DCM-1 patient (CF DCM) and skin fibroblasts from the DCM-1 patient (SF) under light microscopy. Scale bar: 100 μm

3.2.2 Quantification of cell growth

As cardiac fibroblasts are the main cell type in the heart with the ability to grow, the assumption that attaching and growing cells should be cardiac fibroblasts had to be quantified. 500,000 cells were plated on 6 cm cell culture dishes and counted one, two and three days after plating to assess their proliferation capacities (Figure 8).

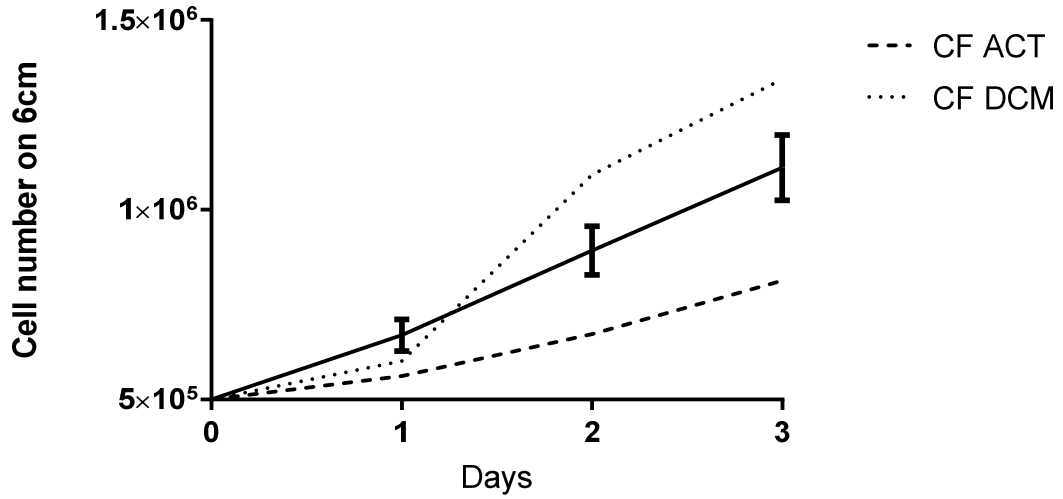

Figure 8: Quantification of cell growth. Proliferation capacity over three days of different human cardiac fibroblasts (n=7), cardiac fibroblasts of the ACT-4 patient (CF ACT) and cardiac fibroblasts of the DCM-1 patient (CF DCM). Cultivation and cell count of the additional cardiac fibroblasts were performed by technician Carmen Klopper.

3.2.3 Gene expression

Next, the cells were analyzed for mRNA expression of general fibroblast markers (Figure 9, A) and markers of cardiac fibroblasts (Figure 9, B) using qRT-PCR. The RNA from the cardiac fibroblast lines of ACT-4, DCM-1 and the healthy control was compared to RNA from induced pluripotent stem cell-derived cardiomyocytes (iPS-CM) and cardiac tissue (myocardium) to further discriminate the isolated cells from cardiomyocytes and to RNA from skin fibroblasts to assure cardiac origin.

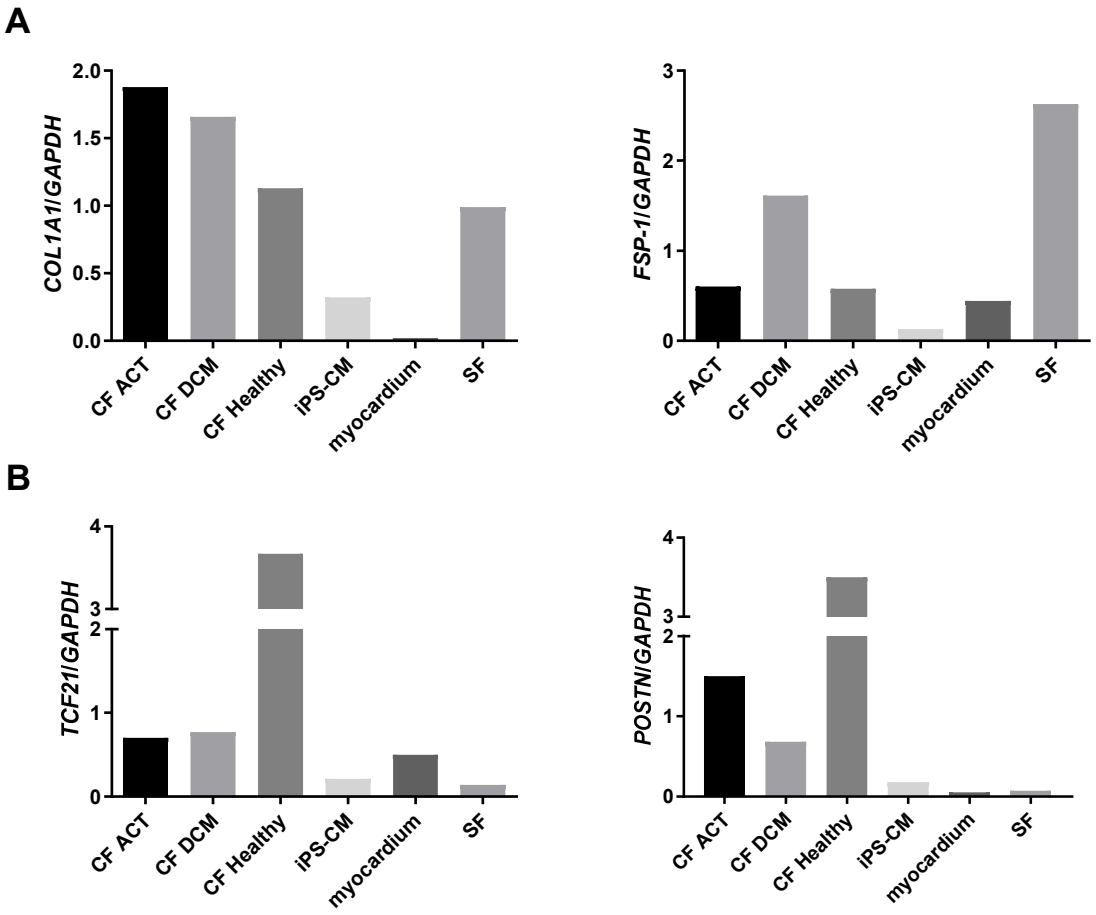

Figure 9: Relative mRNA expression of fibroblast markers. qRT-PCR analysis of cultivated human cardiac fibroblasts from the ACT-4 patient (CF ACT), the DCM-1 patient (CF DCM), cardiac fibroblasts of a healthy control (CF Healthy), iPS-cardiomyocytes (iPS-CM), healthy human heart tissue (myocardium) and cultivated skin fibroblasts of the same DCM-1 patient (SF). *GAPDH* was used as reference gene. **A:** Expression of general fibroblast markers c*ollagen type 1 (COL1A1)* and *fibroblast-specific-protein-1* (*FSP-1)* showing that the isolated cells were fibroblasts. **B:** Expression of markers for cardiac fibroblasts *transcription-factor-21 (TCF-21)* and *periostin (POSTN)* discriminated the fibroblasts to be of the cardiac type.

Cultivated cardiac fibroblasts *in vitro* behave like stressed cardiac fibroblasts *in vivo* with an increase in proliferation and production of extracellular matrix and are hence called myofibroblasts. The combination of *TCF-21* and *POSTN* defines myofibroblasts against other types of fibroblasts.

3.2.4 Immunofluorescence staining

The last method used for characterization was immunocytochemistry. The isolated and cultivated cells were stained for collagen1 (COL1) and α-smooth muscle actin (α-SMA) as proteins typical for fibroblasts (Figure 10). While all of the cells expressed COL1A1, α-SMA was scarcely expressed in the skin fibroblasts. The high levels of α-SMA further point to the cultivated cardiac fibroblasts being myofibroblasts.

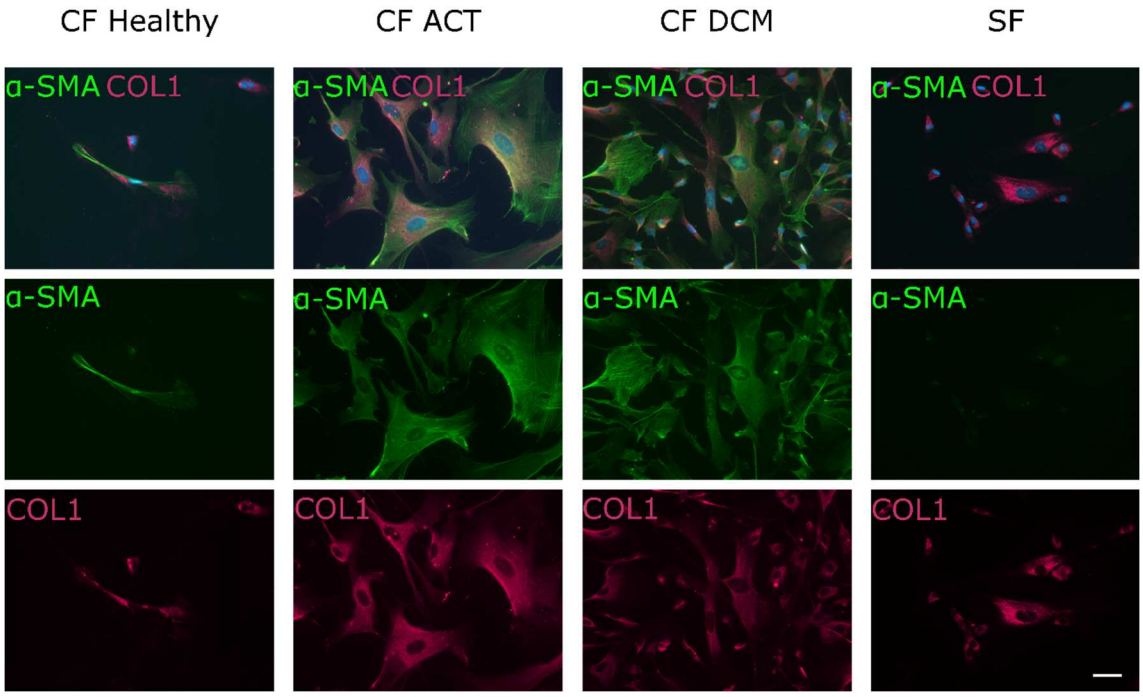

Figure 10: Expression of fibroblast markers on protein level. Immunostaining of healthy cardiac fibroblasts (CF Healthy), cardiac fibroblasts from the ACT-4 patient (CF ACT), cardiac fibroblasts from the DCM-1 patient (CF DCM) and skin fibroblasts from the DCM-1 patient (SF) with antibodies against α-SMA and COL1. DAPI was used for nuclear staining. Scale bar: 50 µm.

To conclude, cells were isolated from fresh human cardiac tissue, cultivated and characterized as cardiac fibroblasts for further experiments.

3.3 NADPH oxidase genotype

As described in 1.1.6, there are three SNPs in different subunits of the NADPH oxidase associated with ACT development that are potentially predisposing. The patient recruitment was done without knowledge of the patient's genotype. To investigate the occurrence of the SNPs in the cardiac fibroblasts (Table 12) and the cardiac tissue (Table 13) and potentially gain insights into effects, the patients were genotyped. Genomic DNA was isolated and used for sequencing (Figure 11).

Table 12: Genotypes of cardiac fibroblasts.

	CYBA	RAC2	NCF4
CF ACT	C**T**	**AA**	**AA**
CF DCM	CC	**AA**	GG
SF Healthy	CC	TT	G**A**

The ACT-4 patient (CF ACT) was heterozygous or homozygous for all three SNPs associated with ACT manifestation, *CYBA* rs54673, *RAC2* rs13058338 and *NCF4* rs8187710 (highlighted in bold). The DCM-1 patient (CF DCM) carried only the SNP for *RAC2*. Meanwhile, skin fibroblasts from a healthy control from a study by Haupt 2018 was homozygous for the wildtype allele in *CYBA* and *RAC2* and heterozygous for *NCF4*.

Table 13: Genotypes of cardiac tissue

	CYBA	RAC2	NCF4
ACT4	C**T**	**AA**	**AA**
ACT5	CC	**AA**	GG
ACT6	C**T**	**AA**	**A**G
ACT7	C**T**	T**A**	GG
ACT8	C**T**	**AA**	**A**G

All five ACT patients (ACT4-8) carried the SNP rs13058338 in *RAC2*, while the SNPs *CYBA* rs54673 and *NCF4* rs8187710 vary between the patients. SNPs associated with ACT manifestation highlighted in bold.

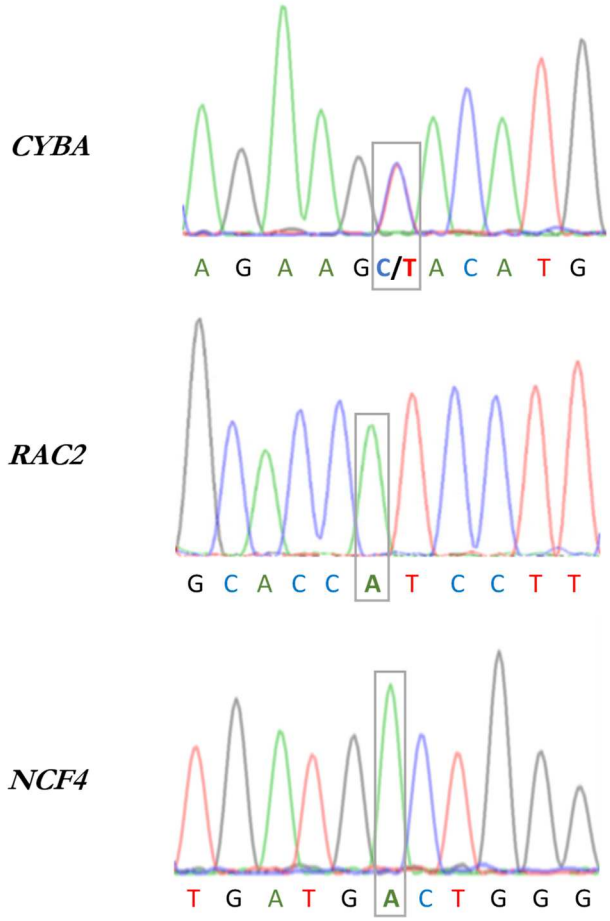

Figure 11: Sequencing chromatograms of cardiac tissue of ACT-4. Genotype of cardiac tissue of patient ACT-4 for the SNPs in *CYBA*, *RAC2* and *NCF4*. Nucleotide of interest framed. Depiction representative for all sequencing data.

In summary, cardiac fibroblasts and cardiac tissue was genotyped for SNPs associated with ACT development in *CYBA*, *RAC2* and *NCF4*.
Three of the five ACT patients were positive for the SNPs in *CYBA* and *NCF4*, while all the ACT patients carried at least one mutated allele for *RAC2*.

3.4 NADPH oxidase subunit expression

Because of the associated SNPs and its role in the production of reactive oxygen species the NADPH oxidase has become a target of ACT research. In this work, the NADPH oxidase subunit expression was investigated using different approaches. Firstly, the immediate effect of DOX treatment on cardiac fibroblasts was analyzed. Secondly, cardiac tissue from patients with end-stage heart failure provided insight into NADPH oxidase subunit expression in the manifested chronic disease.

3.4.1 Acute reaction of human cardiac fibroblasts to DOX treatment

Cultured cardiac fibroblasts of the ACT-4 patient and the DCM-1 patient and skin fibroblasts from the DCM-1 patient as a non-cardiac comparison were treated with DOX concentrations of 0.1 μM and 0.25 μM in human fibroblast medium for 24 hours.

NADPH oxidase subunits *NOX2*, *NOX4*, *CYBA*, *RAC1*, *RAC2* and *NCF4* were analyzed regarding mRNA expression using qRT-PCR (Figure 12). *GAPDH* was used as a reference gene.

For the untreated cells, expression of the subunits *NOX4*, *RAC1*, *RAC2* and *NCF4* was significantly higher in the cardiac fibroblasts compared to the skin fibroblasts. Furthermore, the subunit *NCF4* was expressed significantly more strongly in the cardiac fibroblasts of the ACT-4 patient carrying the SNP compared to the cardiac fibroblasts of the DCM-1 patient without the SNP.

When treated with DOX, the cardiac fibroblasts of both ACT-4 and DCM-1 reacted with a non-significant increase in the expression of *NOX2* and *RAC2*, while the expression of *NOX4* in DCM-1 and *RAC1* in ACT-4 and DCM-1 was non-significantly decreased. *CYBA* expression in the cardiac fibroblasts was decreased at a DOX concentration of 0.1 μM and subsequently increased again at 0.25 μM.

The NADPH oxidase subunit mRNA expression in the skin fibroblasts remained nearly unchanged upon DOX treatment, except for a slight decrease in the expression of the subunits *NOX4*, *RAC1* and *RAC2* at 0.25 μM DOX. The mRNA of the subunits *NOX2* and *NCF4* was not detectable in the skin fibroblasts.

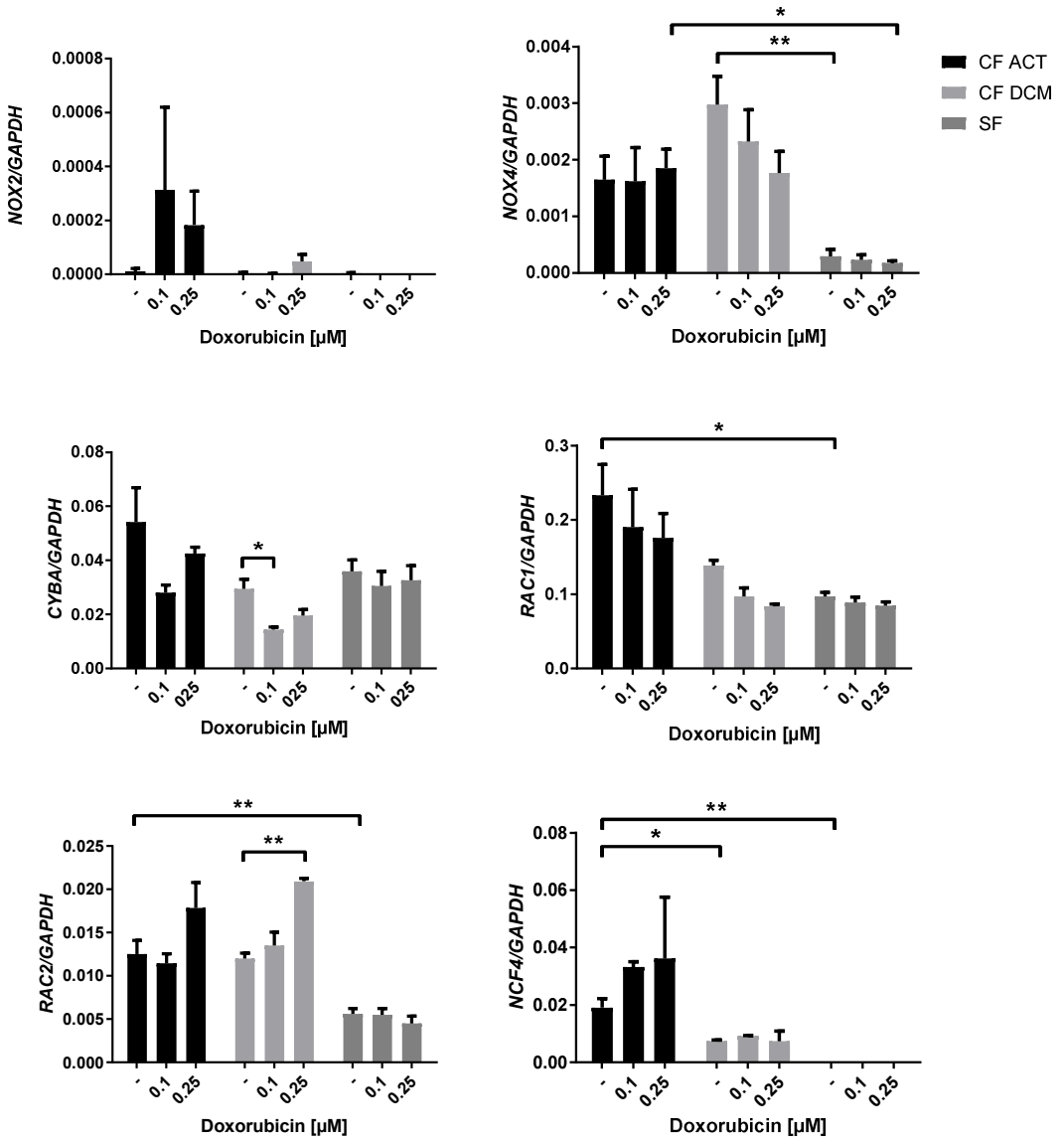

Figure 12: Relative mRNA expression of NADPH oxidase subunits in human fibroblasts. qRT-PCR data for genes *NOX2*, *NOX4*, *CYBA*, *RAC1*, *RAC2*, *NCF4* in cardiac fibroblasts from the ACT-4 patient (CF ACT), cardiac fibroblasts from the DCM-1 patient (CF DCM) and skin fibroblasts from the DCM-1 patient (SF) under basal condition (-) and different concentrations of DOX (0.1 µM and 0.25 µM). n=3 biological replicates (samples from three different passages per cell type) for each measurement.

To study protein expression of the NADPH oxidase subunits in the cardiac and skin fibroblasts, Western blotting was performed with whole cell samples for the subunits NOX4 and RAC2. NOX2 was not detectable in the whole cell protein, but was successfully blotted using membrane fraction samples. The membrane fraction samples were shown in relation to the amount of protein loaded in µg due to varying loads between samples, while GAPDH was used as a reference protein for the whole cell samples.

NOX2 showed a tendency for increased expression after DOX treatment in all analyzed cardiac fibroblasts, although without significance. The expression level overall was lower in the ACT-4 patient compared to the DCM-1 patient. The skin fibroblast reacted to DOX treatment in a similar way, although the increase in expression from 0.1 µM to 0.25 µM DOX concentration was not evident (Figure 13).

NOX4 was significantly decreased in the cardiac fibroblasts of the DCM-1 patient at a DOX treatment concentration of 0.25 µM, while the cardiac fibroblasts of the ACT-4 patient remained nearly unchanged. RAC2 was significantly more highly expressed in the cardiac fibroblasts compared to the skin fibroblasts in the untreated cells, but there was no significant change after DOX treatment (Figure 14).

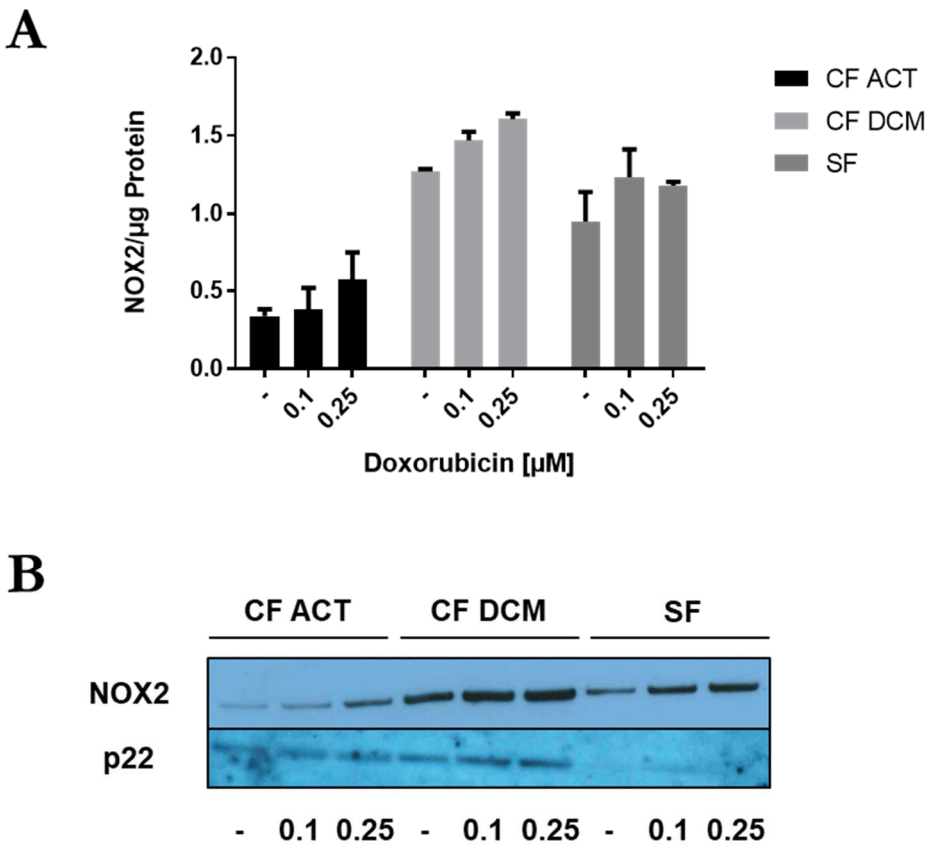

Figure 13: Protein expression of NADPH oxidase subunits in the membrane fraction of human fibroblasts. Western blot analysis of NOX2 in the membrane fraction of cardiac fibroblasts from the ACT-4 patient (CF ACT), cardiac fibroblasts from the DCM-1 patient (CF DCM) and skin fibroblasts from the DCM-1 patient (SF) under basal condition (-) and different concentrations of DOX (0.1 µM and 0.25 µM) for 24h. n=2 biological replicates. **A:** Relative protein expression normalized to the amount of protein loaded. **B:** Western blot image of NOX2 used for quantification and of p22 (n=1).

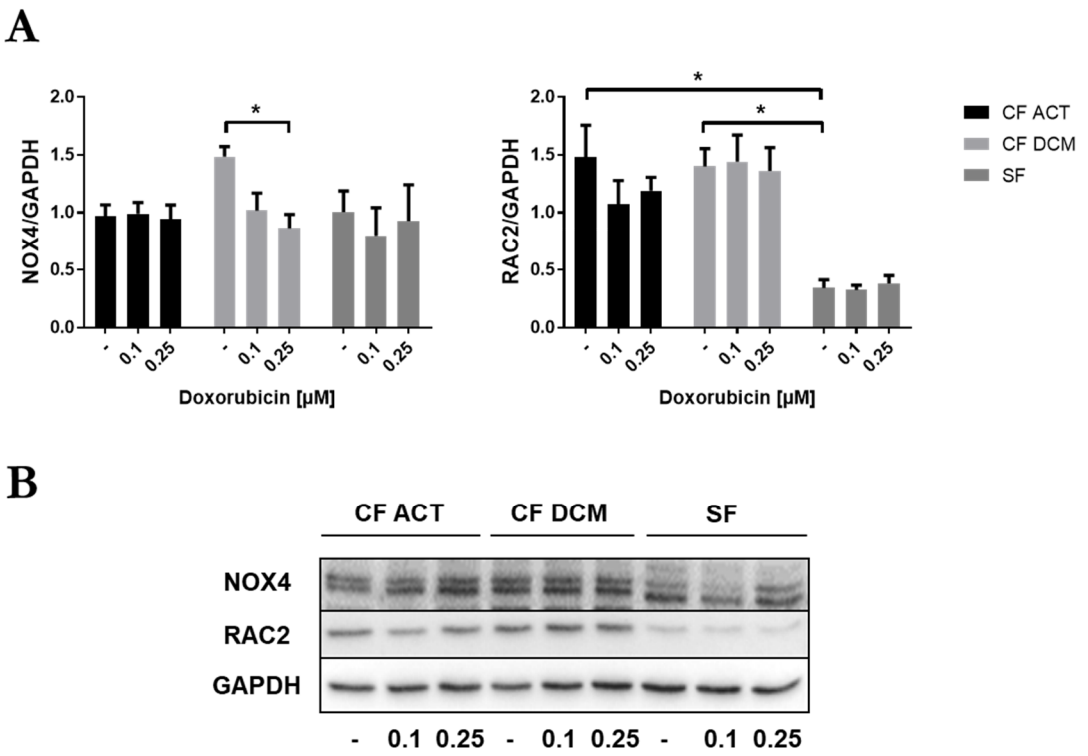

Figure 14: Protein expression of NADPH oxidase subunits in human fibroblasts. Western blot analysis of NOX4 and RAC2 in cardiac fibroblasts from the ACT-4 patient (CF ACT), cardiac fibroblasts from the DCM-1 patient (CF DCM) and skin fibroblasts from the DCM-1 patient (SF) under basal condition (-) and different concentrations of DOX (0.1 µM and 0.25 µM) for 24h. n=3 biological replicates. **A:** Relative protein expression normalized to GAPDH as a reference protein. **B:** Western blot images used for quantification.

In conclusion, NADPH oxidase subunit expression was analyzed in cardiac and skin fibroblasts on mRNA and protein level. Subunits RAC2 and NCF4 were expressed significantly more highly in the cardiac fibroblasts compared to the skin fibroblasts.
As an immediate response to DOX treatment, there is an increase in the expression of NOX2 on protein and mRNA level in the ACT patient. NOX4 was downregulated on protein and mRNA level in the DCM patient, while no change was found in the ACT patient.

3.4.2 Cardiac tissue of patients with end-stage heart failure

As the critical form of ACT manifests itself as chronic heart failure, a later time point in disease progression is also of interest for investigation. Therefore, the expression of NADPH oxidase subunits in patients with end-stage heart failure receiving heart transplantation therapy was also investigated. Left ventricle tissue of five patients with a

dilative cardiomyopathy after anthracycline chemotherapy, three patients with a dilative cardiomyopathy of other origins and three healthy controls was analyzed for expression of NADPH oxidase subunits *NOX2*, *NOX4*, *CYBA*, *RAC1*, *RAC2, NCF1, NCF2* and *NCF4* on mRNA level (Figure 15). *GAPDH* was used as a reference gene.

In comparison to the healthy controls, the expression of subunits *NOX2*, *RAC1*, *RAC2*, *NCF1*, *NCF2* and *NCF4* were all, although non-significantly, decreased in the patients with ACT, while they were increased in the patients with a DCM of other origins. In contrast, *NOX4* and *CYBA* were non-significantly increased in the ACT patients when compared to the healthy controls.

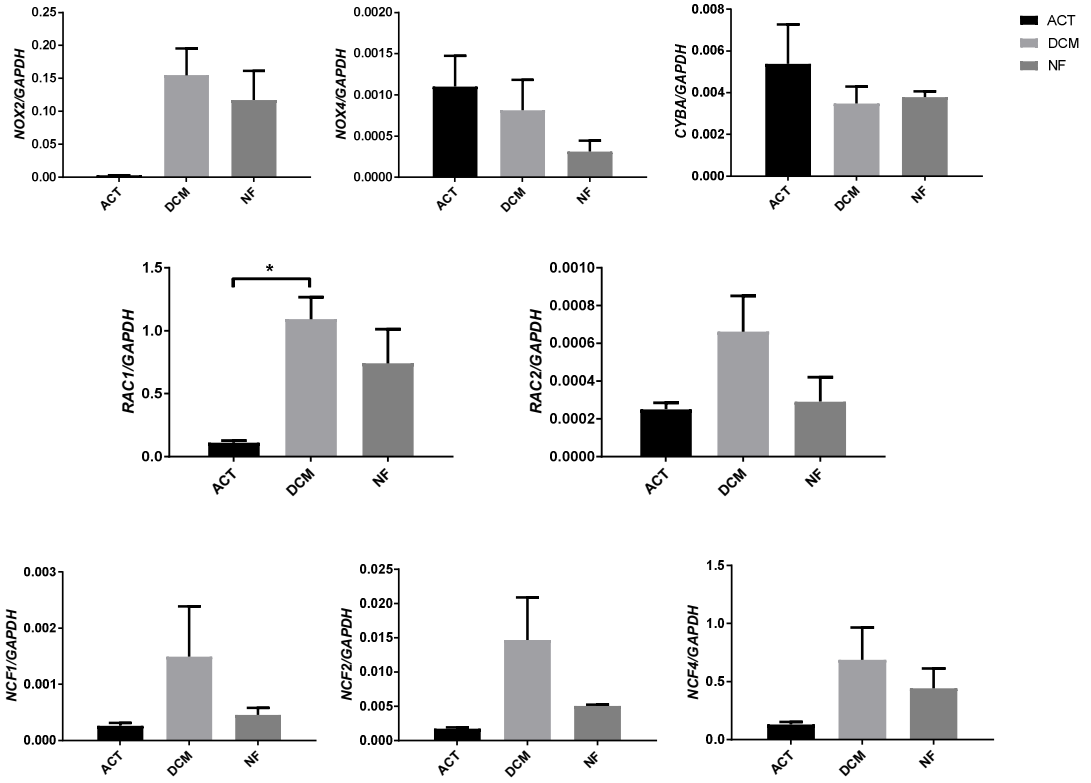

Figure 15: Relative mRNA expression of NADPH oxidase subunits in human cardiac tissue. qRT-PCR data for genes *NOX2*, *NOX4*, *CYBA*, *RAC1*, *RAC2*, *NCF1*, *NCF2* and *NCF4* in human cardiac tissue of ACT patients (ACT, n=5), DCM patients (DCM, n=3) and healthy non-failing controls (NF, n=3). *GAPDH* was used as a reference gene.

Protein expression was also studied in whole cardiac tissue with Western blotting for NOX2, NOX4 and RAC2 (Figure 16). As the Western blot images for NOX2 showed lots of unspecific bands, they were not used for analysis.

NOX4 expression was again increased in the ACT patients when compared to DCM patients and healthy controls. RAC2 expression was decreased in ACT and DCM patients compared to the healthy controls.

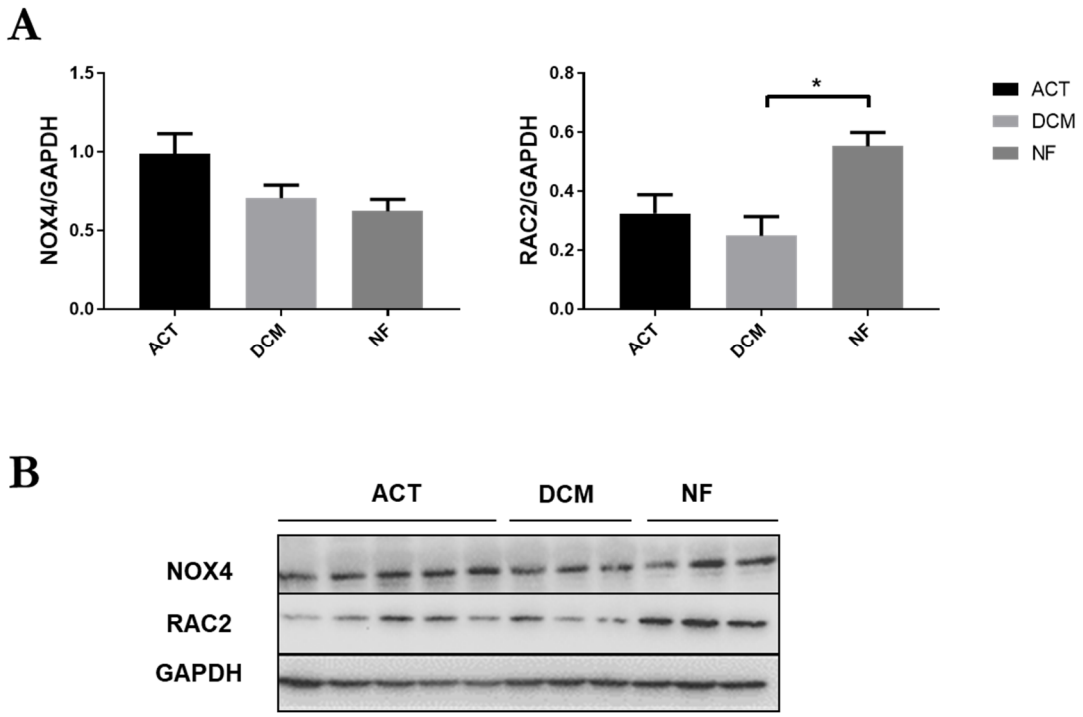

Figure 16: Protein expression of NADPH oxidase subunits in human cardiac tissue. Western blot analysis of NOX4 and RAC2 in human cardiac tissue of ACT patients (ACT, n=5), DCM patients (DCM, n=3) and healthy non-failing controls (NF, n=3). GAPDH was used as a reference protein. **A:** Relative protein expression normalized to GAPDH as a reference protein. **B:** Representative Western blot images used for quantification.

In summary, NADPH oxidase subunit expression was analyzed in human cardiac tissue on mRNA and protein level. Expression levels for the subunits differ between ACT patients, DCM patients and healthy controls.

3.5 DOX-triggered production of ROS in human cardiac fibroblasts

The previously investigated NADPH oxidase is an enzyme complex producing different species of ROS. As described in 1.1.5.1, the production of ROS leading to oxidative stress is discussed as one of the main pathomechanisms leading to ACT manifestation. Therefore, to explore a potential role of cardiac fibroblasts in ACT development, ROS production upon DOX treatment in the human cardiac fibroblasts was investigated in this project.

3.5.1 Extracellular hydrogen peroxide production

Cardiac fibroblasts of the ACT-4 and the DCM-1 patient and skin fibroblasts from the DCM-1 patient were treated with 0.1 μM, 0.25 μM and 1 μM DOX in human fibroblast medium for 24 hours, respectively. Extracellular H_2O_2 levels were then assessed using the Amplex Red Peroxidase Assay (Figure 17).

The amount of H_2O_2 in the supernatant is dependent on the number of cells. Consequently, for an ideal measurement every condition and cell line should have the same number of cells. This was not feasible, because the human fibroblasts proliferate in different rates depending on cell line and treatment intensity. To address this problem, a replica of the experiment was run simultaneously and used to quantify the cell count instead of measuring ROS production. This data was used to normalize ROS levels to the number of cells.

H_2O_2 production in the untreated human fibroblasts was significantly higher in the cardiac fibroblasts compared to the skin fibroblasts. Furthermore, the cardiac fibroblasts of the ACT-4 patient produced significantly higher amounts than the cardiac fibroblasts of the DCM-1 patient (Figure 17, A).

Upon DOX treatment all fibroblasts reacted with a significant increase in H_2O_2 production with rising DOX concentrations of up to 0.25 μM, while at a concentration of 1 μM H_2O_2 production went down again, suggesting an apoptotic effect of DOX treatment at 1 μM (Figure 17, B). Peak H_2O_2 levels at 0.25 μM Dox were significantly higher in the cardiac fibroblasts of the ACT-4 patient compared to the cardiac fibroblasts of the DCM-1 patient and the skin fibroblasts (Figure 17, A).

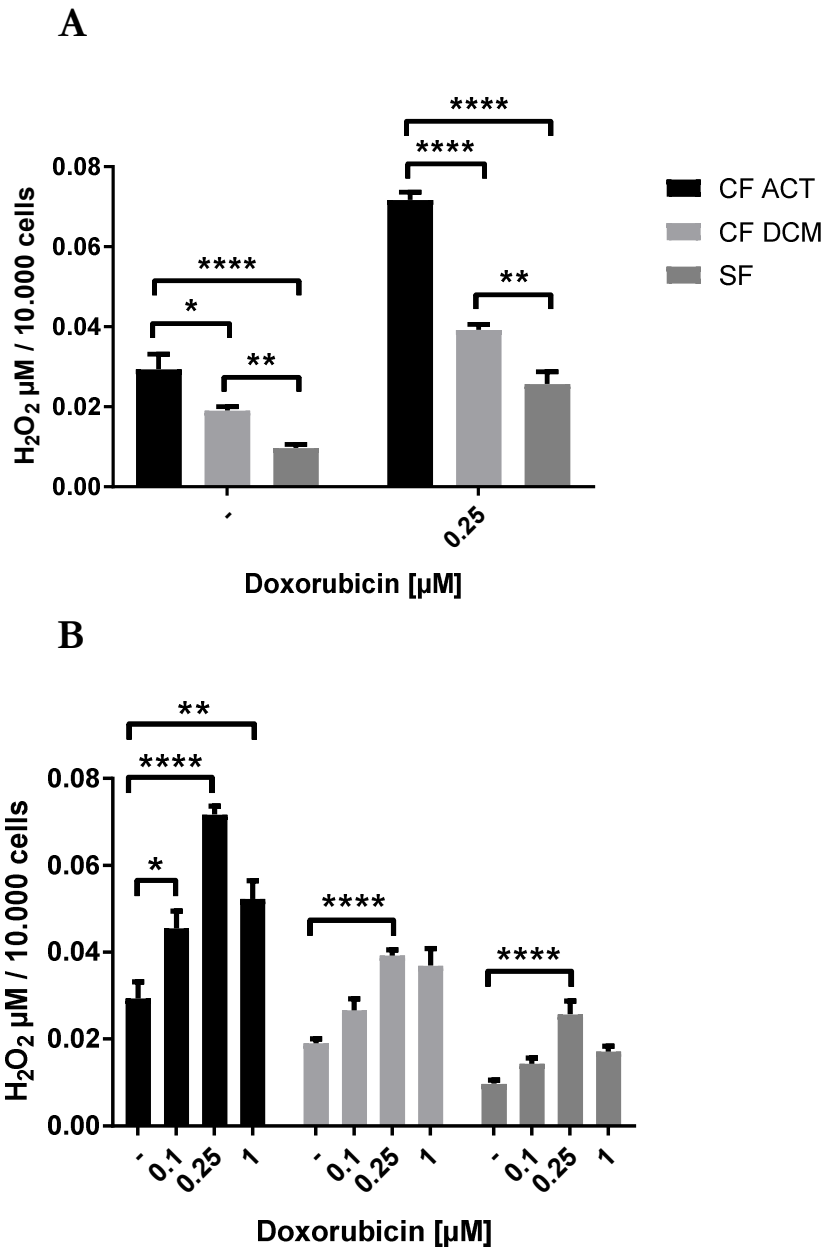

Figure 17: Extracellular H_2O_2 production of human fibroblasts. Relative Amplex Red Assay data for cardiac fibroblasts from the ACT-4 patient (CF ACT), cardiac fibroblasts from the DCM-1 patient (CF DCM) and skin fibroblasts from the DCM-1 patient (SF) under basal condition (-) and different concentrations of DOX (0.1 µM, 0.25 µM, 1 µM). Number of cells was used for normalization. n=3 biological replicates for each measurement.

In conclusion, extracellular H_2O_2 production was measured in human fibroblasts upon DOX treatment. The production of H_2O_2 was increased until 0.25 µM DOX. Also, H_2O_2 levels were higher in cardiac fibroblasts compared to skin fibroblasts.

3.5.2 Superoxide production in the membrane fraction

Cardiac fibroblasts of the ACT-4 patient and the DCM-1 patient and skin fibroblasts from the DCM-1 patient were once again treated with 0.1 μM and 0.25 μM DOX for 24 hours in HFBM and subsequently separated into the different cell fractions. The membrane fraction was then used to assess superoxide production using the turnover of DHE to 2-EOH measured by HPLC (see 2.2.8) (Figure 18).

To ensure equal cell numbers for the different treatment conditions and cell lines, measured growth rates of the different cell lines and treatment conditions from the Amplex Red Assay experiment were used to calculate the number of cells that needed to be plated for equal cell numbers after treatment. SOD was used as a superoxide scavenger to confirm test specifity for the measurement of superoxide. The signal of 2-EOH was significantly decreased to near baseline in the presence of SOD, independent of the used concentrations of DOX.

Superoxide production was increased upon DOX treatment in the cardiac and skin fibroblasts. The highest increase was found in ACT-4 with a 3-fold induction after 0.25 μM of DOX compared to basal conditions. In DCM-1 we found a 2-fold increase of superoxide production, whereas SF showed a low increase after DOX treatment. Of note, the variance in signal strength was high in skin fibroblasts resulting in high standard errors of the mean.

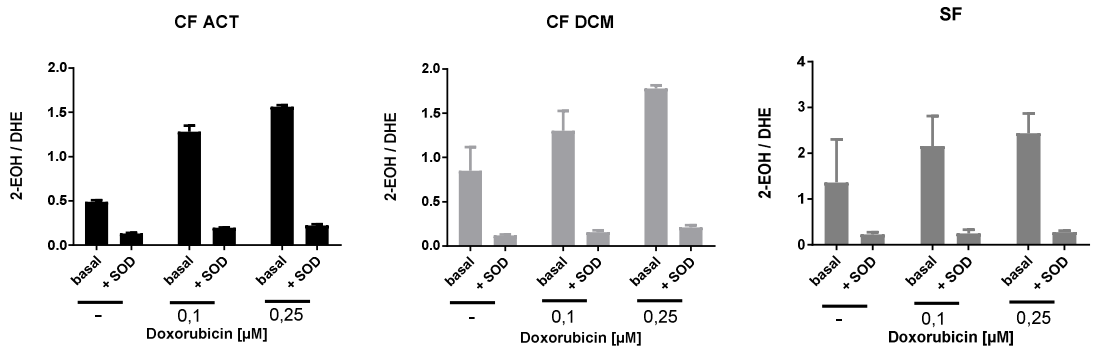

Figure 18: Superoxide production in the membrane fraction of human fibroblasts. HPLC measurements of 2-EOH and DHE production as a marker of superoxide levels in membrane fractions of ACT-4 cardiac fibroblasts (CF ACT), DCM-1 cardiac fibroblasts (CF DCM) and skin fibroblasts from DCM-1 (SF) under basal condition (-) and after doxorubicin treatment (0.1 µM, 0.25 µM). Each treatment condition was also measured with superoxide dismutase (SOD) as a negative control. n=2 biological replicates for each measurement.

By measuring 2-EOH production with and without NADPH in the incubation mix with DHE it was possible to assess the relative NADPH contributable amount of superoxide (Figure 19). Strikingly, NADPH appeared to not play a role in superoxide production in the untreated cells, but only contributed upon DOX treatment. This was detectable for cardiac and skin fibroblasts without measurable differences between the two groups. This data suggests that the NADPH oxidase 2 becomes activated after cells are treated with DOX.

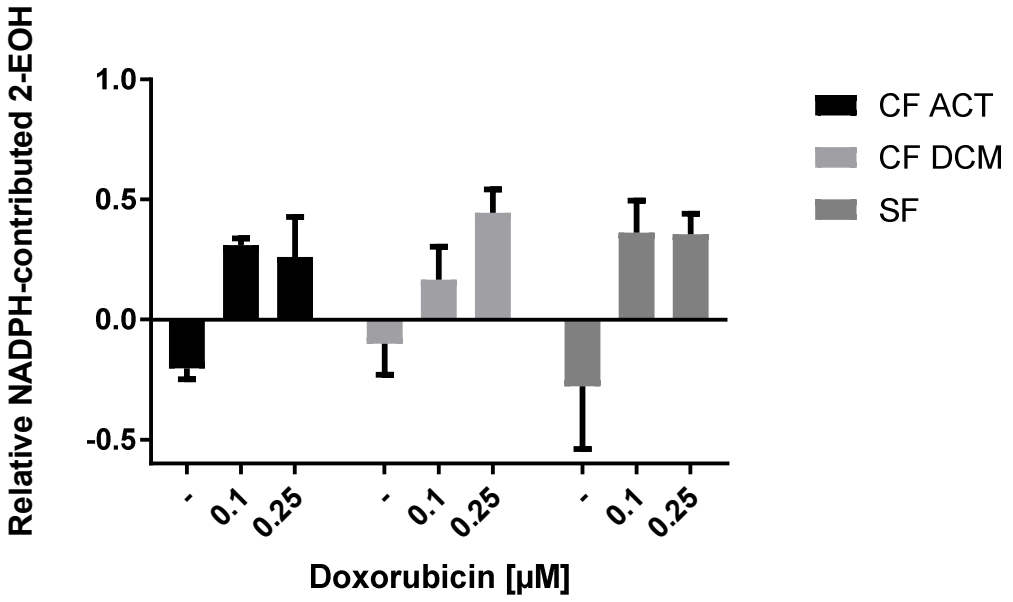

Figure 19: NADPH contributable superoxide production in the membrane fraction of human fibroblasts. Relative NADPH-contributed 2-EOH production as a marker for superoxide levels in membrane fractions of ACT-4 cardiac fibroblasts (CF ACT), DCM-1 cardiac fibroblasts (CF DCM) and skin fibroblasts from DCM-1 (SF) under basal condition (-) and different concentrations of doxorubicin (0.1 µM, 0.25 µM). n=2 biological replicates for each measurement.

To summarize, superoxide production was assessed in the membrane fraction of human fibroblasts upon DOX treatment. DOX lead to an increase in superoxide levels. Meanwhile, NADPH contributable superoxide production was only measurable when triggered with DOX treatment.

4 Discussion

Patients receiving anthracycline chemotherapy are highly impaired in their outcome by the momentous side effect of anthracycline-induced cardiotoxicity. ACT is a cumulative, dose-dependent damage of the heart leading to symptomatic heart failure in 6 to 9 % of all patients (Lotrionte et al. 2013; Cardinale et al. 2015). The symptomatology ranges from a slight reduction of left ventricular ejection fraction to end-stage heart failure in the form of dilative cardiomyopathy (Rahman et al. 2007). Preventive and therapeutic strategies are scarce due to a lack of knowledge about molecular mechanisms causing cardiotoxicity. The creation of ROS, inhibition of TOP2ß and mitochondrial dysfunction have been reported to cause the histopathological changes including cardiomyocyte apoptosis, myofibril loss and cardiac fibrosis (Unverferth et al. 1983; Doroshow et al. 1985; Lebrecht et al. 2005; Ichihara et al. 2007; Lyu et al. 2007). Another research target is the NADPH oxidase, as it is a major player in ROS production and ACT-associated SNPs have been found in three different subunits of the enzyme complex (Wojnowski et al. 2005). So far, most studies used animal models and focused on cardiomyocytes leaving out non-cardiomyocyte cells in the highly complex and multifactorial development of ACT. Cardiac fibroblasts are the largest non-cardiomyocyte population in the heart and an increasing number of functions in homeostasis and heart damage are being reported (Weber et al. 2013). Recent studies even suggested a role in ACT manifestation (Zhang et al. 2016). The aim of this thesis was to investigate the contribution of cardiac fibroblasts to the development of ACT in terms of NADPH oxidase subunit expression and ROS production.

Human cardiac fibroblasts of an ACT patient and a DCM patient were isolated from human cardiac tissue of freshly transplanted hearts and characterized in morphology, proliferation and expression of fibroblast markers on mRNA and protein level in order to be used for ACT research.

The cells were then analyzed for NADPH oxidase subunit expression on mRNA and protein level upon DOX treatment. Subunits RAC2 and NCF4 were expressed significantly more strongly in the cardiac fibroblasts compared to the skin fibroblasts. As an immediate response to DOX treatment, there was an increase in the expression of NOX2 on protein and mRNA level in the ACT patient. NOX4 was downregulated on protein and mRNA level in the DCM patient, while no change was found in the ACT patient.

Also, ROS production was analyzed upon DOX treatment using the Amplex Red assay for the measurement of extracellular hydrogen peroxide production and the DHE-HPLC assay for the measurement of superoxide production of the membrane fraction. Production of H_2O_2 was increased until a concentration 0.25 μM DOX and baseline H_2O_2 levels were higher in cardiac fibroblasts compared to skin fibroblasts. DOX treatment also lead to an increase in superoxide levels and NADPH contributable superoxide production was only measurable when triggered with DOX treatment.

Additionally, cardiac tissue from ACT and DCM patients was used to assess the degree of fibrosis and expression of NADPH oxidase subunits in end-stage heart failure compared to healthy controls. ACT and DCM patients showed significantly larger fibrotic areas compared to healthy control tissue and expression levels for the subunits differed between ACT patients, DCM patients and healthy controls.

4.1 Fibrosis in human cardiac tissue from ACT patients, DCM patients and controls

To characterize the disease phenotype of the tissue used for analysis as well as to establish the necessity of investigating cardiac fibroblasts, the degree of fibrosis was analyzed in human cardiac tissue of ACT patients, DCM patients and healthy non-failing controls. The sliced tissue was stained with Masson's trichrome staining and areas of fibrosis were quantified by virtual microscopy.

The increased areas of fibrosis in ACT and DCM patients compared to healthy controls found in this study accord with early disease phenotype depictions by Unverferth et al. 1983 and Doroshow et al. 1985. The proposed histopathological changes have been widely accepted in the field of ACT research. Still, most studies investigating ACT have focused on the cardiomyocyte as the functional cell in the heart and its response to DOX treatment, while the effect of anthracyclines on cardiac fibroblasts and other non-myocyte cells of the heart remains unclear. Fibrotic remodeling of the myocardium may be a key part of ACT development and lead to the described end-stage heart failure in the form of dilative cardiomyopathy as fibrosis impairs cardiac function and contractility.

The increase of mean fibrotic areas in ACT tissue to 24.2 % and 23 % in DCM tissue from 8.5 % in the healthy heart roughly concur with results found by investigating human endomyocardial biopsies from patients with DCM showing 18.7 % in patients against 13 % in healthy controls (Di et al. 2000). The degree and distribution of fibrotic areas appear to be similar in the groups of ACT and DCM patients. Considering the fibrotic phenotype of ACT, the investigation of fibroblasts seems worthwhile.

4.2 Isolation and characterization of human cardiac fibroblasts

To investigate the working hypothesis that cardiac fibroblasts contribute to ACT development via ROS production and react to anthracycline treatment with expression changes of the NADPH oxidase subunits, the establishing of a cell culture platform was necessary. Cells isolated from left ventricle tissue needed to be characterized to substantiate the assumption of being cardiac fibroblasts.

The cells used in this study showed morphological characteristics of fibroblasts such as large, roughly triangular cell bodies, big nuclei and irregular cell protrusions connecting the cells (Figure 7). These qualities speak against other cell types of the heart like endothelial cells, which are small and fusiform to polygonal, and cardiomyocytes, which are thin and elongated (Cormack 2001). Proliferation can also be counted to fibroblast characteristics and was quantifiable for all of the cells used (Figure 8).

There are various markers that have been reported to be specific for fibroblasts in general or cardiac fibroblasts specifically. In this study, *FSP-1* and *COL1* have been used to ensure the fibroblast cell type against cardiomyocytes, while *a-SMA*, *TCF-21* and *POSTN* were used to differentiate cardiac fibroblasts against fibroblasts in general (Figure 9).

FSP-1 and *COL1* were highly expressed in the isolated cardiac fibroblasts and the healthy cardiac fibroblasts (Figure 9). This is in line with published work by Strutz et al. 1995, who have shown that the mRNA expression of *FSP-1* distinguished the fibroblasts from cardiomyocytes. Furthermore, *COL1* was expressed on mRNA and protein level in the fibroblasts, as expected (Zeisberg et al. 2007).

In contrast to other types of fibroblasts, the differentiation of cardiac fibroblasts can be difficult at times. A gene that was reported to have a high expression in cardiac fibroblasts is *TCF-21* (Kanisicak et al. 2016). The expression levels found in this study underline the assumption of the isolated cells being cardiac fibroblasts when compared to the commercial cardiac fibroblasts and skin fibroblasts. As described in 1.2.1, cardiac fibroblasts turn into myofibroblasts when cultured in vitro. Early on, an increase in α-SMA expression was found for the activated cardiac fibroblasts (Leslie et al. 1991) and the immunocytochemistry pictures from this study show α-SMA to be expressed more highly in cardiac fibroblasts than in skin fibroblasts (Figure 10). Kaur et al. 2016 reported *POSTN* to be a superior marker compared to *a-SMA* and other tested genes for the myofibroblast cell type. The analysis in this study substantiates this claim as *POSTN* expression was high in the cultured cardiac fibroblasts, but very low in skin fibroblasts or cardiomyocytes.

Consequently, the isolated cells were declared cardiac fibroblasts for further experiments in ACT research. Furthermore, these data suggest that genes *TCF-21* and *POSTN* are suitable to differentiate cardiac fibroblasts from skin fibroblasts.

4.3 NADPH oxidase SNPs

The unexplained high interindividual variance in ACT manifestation might be related to genetic predisposition. The associated SNPs in the NADPH oxidase subunits *CYBA*, *RAC2* and *NCF4* evaluated by the meta-analysis of Leong et al. 2017 are among the most promising gene variants. However, Wojnowski et al. 2005 also concluded that, while statistical relevance is given, the low specificity of the SNPs restricts pretherapeutic risk stratification via genotype diagnosis as the potential of unjustly depriving patients of possibly life-saving anthracycline therapy is too high. On the other hand, further investigation of functional consequences of the associated genetic variants might provide insights into molecular mechanisms contributing to ACT development.

The small number of patients included in this study limits any conclusion about the validity of allele distribution found (Table 12 and Table 13). The patient material was obtained without knowledge of genotype and it is notable that nearly all patients were homozygous for the potentially predisposing SNP in the NADPH oxidase subunit *RAC2* even though the homozygous frequency in the German population was reported at 15 %. Additionally, nearly all patients carried the SNP in *CYBA* with a SNP frequency in the German population of 55 % (Wojnowski et al. 2005). The SNP in *NCF4* was found in four out of six ACT patients, supporting the conflicting results of statistical relevance found in a lot of studies included by Leong et. al. 2017.

In conclusion, the genotyping results found in this study resemble preliminary gene studies in similar ACT cohorts (Wojnowski et al. 2005; Reichwagen et al. 2015; Leong et al. 2017). Genotype differences between the patients can be taken into consideration when interpreting the results of expression analysis and ROS production, although more conclusive data about functional consequences of the SNPs for enzyme activity is pending.

4.4 NADPH oxidase subunit expression

4.4.1 Human cardiac fibroblasts

The working hypothesis that human cardiac fibroblasts play a distinct role in ACT development through the NADPH oxidase was investigated by NADPH oxidase subunit

expression analysis. To our knowledge, this is the first study of the NADPH oxidase subunits in human cardiac fibroblasts in anthracycline treatment.

When comparing expression levels in the untreated cells, there were significant differences between the cardiac fibroblasts and the skin fibroblasts (Figure 12 and Figure 14). The subunit *RAC2* was expressed significantly more highly on protein and mRNA level in cells from cardiac origin, which was also found for *NCF4* on mRNA level. The subunit *NOX4* showed a significantly higher expression in cardiac fibroblasts on mRNA level, but was similarly expressed in all cell types on protein level. These findings might indicate variations in NADPH oxidase function in different types of fibroblasts. For example, Cucoranu et al. 2005 reported that fibroblast transition into myofibroblasts by transforming growth factor-ß1 might be mediated by the NADPH oxidase 4. Further insights into NADPH oxidase function in cardiac fibroblasts are pending.

Additionally, *NCF4* expression on mRNA level was significantly more strongly in cardiac fibroblasts from the ACT patient carrying both alleles with the SNP associated with ACT than in the cardiac fibroblast of the DCM patient without the SNP. This concurs with a publication of Schirmer et al. 2008, which reported a significantly higher expression of the subunits *RAC2* and *NCF4* in leukocytes of donors with the ACT-associated allele of the RAC2 SNP described in this study. The difference in expression in fibroblasts could possibly contribute to the reported association of the SNP with cardiac fibrosis (Cascales et al. 2013). However, as functional consequences of the mutation are not fully understood, additional investigation is needed.

The cells were also treated with 0.1 μM and 0.25 μM DOX for 24 hours to study the acute reaction to anthracycline treatment. The expression of subunit *NOX2* was increased upon treatment. The cardiac fibroblasts showed an increase on mRNA level, while both cardiac and skin fibroblasts showed an increase on protein level. The increased expression of *NOX2* might indicate that the catalytic subunit contributes to heart damage through cardiac fibroblasts. These data are in line with a previous study by Zhao et al. 2010 showing *NOX2* and *NOX4* upregulated after DOX treatment in mice heart tissue. The contribution of *NOX2* to various pathomechanisms of heart failure including cardiac fibrosis has preliminarily been resumed by Zhang et al. 2013. The data from this study suggests this might be in part through direct enzyme regulation in the cardiac fibroblasts.

The subunit *RAC2* was significantly increased in the cardiac fibroblasts after DOX treatment, but not in the skin fibroblasts on mRNA level, although this effect was not found on protein level. So far, increased activity in heart failure has only been described for

RAC1 (Maack et al. 2003). The role of *RAC2* outside of leukocytes is still up to debate. However, the associated SNP in the subunit indicates *RAC2* being important in one way or the other.

Also, the subunit *NCF4*, encoding p40phox, was increasingly expressed upon treatment in the cardiac fibroblasts. The consequence of this finding is unclear, as the function of *NCF4* has been reported to be depending on phosphorylation and subunit interaction (Fan et al. 2009). P40phox is part of the NADPH oxidase and its function is controversially discussed in the literature. Brandes et al. 2014 described that phosphorylation of p67phox and an activation of RAC1/2 is required for activation of NOX2. Phosphorylated p47phox supports the binding of p67phox to NOX2, but in absence of p47phox, p40phox has been reported to activate NOX2 expression (Fan et al. 2009). However, this DOX-induced increase of NCF4 might be associated to the reported association of the *NCF4* SNP with cardiac fibrosis (Cascales et al. 2013).

Lastly, the subunit *NOX4* was decreasingly expressed on mRNA and protein level upon treatment in the cardiac fibroblasts of the DCM patient. However, this effect was not evident in the cardiac fibroblast of the ACT patient. As mentioned before, NOX4 has been described to mediate myofibroblast activation (Cucoranu et al. 2005). The lack of decrease of *NOX4* expression might indicate that the cardiac fibroblasts of the ACT patient are being activated.

As anthracycline treatment effects transcription, it might also be worth to investigate NADPH oxidase subunit expression in human cardiac fibroblasts upon mechanical stress for it might provide insight into fibroblast behavior in the development of delayed chronic ACT. Furthermore, the effect of subunit expression on enzyme activity and potential consequences needs to be studied further to properly understand the role of the NADPH oxidase in cardiac fibroblasts in ACT. All in all, this study showed tendencies of expression changes for NADPH oxidase subunits making the enzyme complex a promising target for ACT research in cardiac fibroblasts.

4.4.2 End-stage heart failure tissue

The analysis of NADPH oxidase subunit expression in tissue of end-stage heart failure patients diagnosed as either ACT or DCM provided insights into different time points of the disease (Figure 15 and Figure 16). It has to be noted though that both mRNA as well as protein was isolated from whole tissue samples. Therefore, potential disturbances of the

measurement due of leukocyte infiltration in the myocardium have to be considered and the results evaluated accordingly.

Interestingly, while the mRNA expression of the subunits *NOX2, RAC1, RAC2, NCF1, NCF2* and *NCF4* was elevated in DCM patients compared to healthy controls, as reported for example by Kuroda and Sadoshima 2010, the expression was decreased in the ACT patients. These findings imply that the NADPH oxidase subunit might behave differently in the development and manifestation of ACT compared to dilative cardiomyopathies of other origins. Especially the strikingly low expression of *NOX2* in the ACT patients is surprising, as the subunit has been reported to contribute to ACT manifestation via ROS production (Zhao et al. 2010). A possible explanation might be that following stimulation of *NOX2* activity during acute ACT-induced cardiac damage, the subunit is subsequently downregulated in expression in the end-stage heart failure phenotype.

Contrary, *NOX4* is expressed more highly in the tissue of the ACT and DCM patients compared to healthy controls on protein and mRNA level. As the NADPH oxidase 4 is constitutively active and therefore upregulated by expression this might mean higher hydrogen peroxide levels in the cardiac tissue of ACT patients. The extended degree of fibrosis in ACT and DCM tissue is possibly mediated by the NADPH oxidase 4 (Cucoranu et al. 2005).

Since *RAC1* and *RAC2* show a reduced expression in ACT and DCM cardiac tissue compared to healthy controls, but are highly expressed in cFBs of the ACT and DCM patients, the main function seems to be associated to cFBs instead of cardiomyocytes.

Ultimately, this study found differences in expression levels for the NADPH oxidase subunits between ACT patients, DCM patients and healthy controls. Unfortunately, the production of ROS was not measurable in frozen tissue, but would be a promising target to study for oxidative stress levels in chronic ACT. This might support the hypothesis from Carvalho et al. 2014 of a cycle of cardiac damage with mitochondrial DNA damage and ROS production.

4.5 Production of ROS in human cardiac fibroblasts upon anthracycline treatment

When investigating the involvement of human cFBs in the development of ACT, the production of ROS as a major pathomechanism has to be evaluated. Due to their high reactivity, short lifespan and fluent conversion into each other the measurement of reactive

oxygen species is challenging. This study used the Amplex Red assay for extracellular hydrogen peroxide and DHE-HPLC for superoxide production in the membrane fraction. The approach had the advantage of a possible connection to the NADPH oxidase data discussed earlier, as hydrogen peroxide is produced by the NADPH oxidase 4 and superoxide is produced by the NADPH oxidase 2. Ultimately, the working hypothesis should be evaluated whether human cFBs differ from other kinds of fibroblasts in their reaction to anthracycline treatment and whether cFBs from the ACT patient are more sensitive to anthracyclines than cFBs from the DCM patient. The measurement of anthracycline-induced ROS production in human cardiac fibroblasts was, to our knowledge, performed for the first time in this study.

4.5.1 Extracellular hydrogen peroxide production

Upon DOX treatment the fibroblasts showed a significant increase in hydrogen peroxide production up to a DOX concentration of 0.25 μM (Figure 17). At 1 μM the hydrogen peroxide level was decreased likely due to increased cell death at supratherapeutic concentrations and the subsequent lack of functioning cell organelles. These data contradict results found by Burridge et al. 2016, who worked with stem cell-derived cardiomyocytes and found hydrogen peroxide levels to be increased with rising DOX concentrations even above 1 μM. Previously, we were able to show that stem cell-derived cardiomyocytes from ACT patients are able to produce increasing H_2O_2 levels up to DOX concentrations of 0.5 μM (unpublished data). The increase in extracellular hydrogen peroxide might lead to fibroblast activation via ROS signaling, damage to the ECM and disturbed ROS signaling in cardiomyocytes.

The levels of hydrogen peroxide were significantly higher in cardiac fibroblasts compared to skin fibroblasts. These data are in line with the mRNA expression of the *NOX4* subunit (Figure 12) and support the idea of the NADPH oxidase 4 having a cardiac specific role in the fibroblasts. Furthermore, this study implies that cardiac fibroblasts from the ACT patient are more sensitive to anthracycline treatment than cardiac fibroblasts from the DCM patient in terms of hydrogen peroxide production. Burridge et al. 2016 as well as preliminary data from our group reported similar results in stem cell derived cardiomyocytes of ACT patients and controls. Due to the limited number of patients used in this study, this trend needs further investigation with larger sample numbers. Still, the implications resulting from this study back up the working hypothesis.

4.5.2 Superoxide production in the membrane fraction

The NADPH oxidase 2 is a major source of superoxide in the cell and is located in the plasma membrane. Therefore, to improve superoxide measurement, the cells were separated into the different organelle fractions. The membrane-enriched fraction was then used to assess superoxide production upon anthracycline treatment.

The fibroblasts reacted to anthracycline treatment of 0.1 μM and 0.25 μM with an increase in superoxide production. The highest increase was found in the cardiac fibroblasts of the ACT patient with a 3-fold induction after 0.25 μM of DOX compared to basal conditions. In the cardiac fibroblasts of the DCM patient, we found a 2-fold increase of superoxide production, whereas the skin fibroblasts showed a low increase after DOX treatment. Furthermore, by incubating the membrane fractions with and without NADPH, it was shown that NADPH-contributable superoxide production was only induced upon DOX treatment. It is therefore likely that the increase in superoxide levels stems from an activation of the NADPH oxidase 2. This particular NADPH oxidase 2-derived ROS has been reported to facilitate several pathomechanisms of contractile dysfunction and cardiac remodeling in ACT manifestation (Zhao et al. 2010). Furthermore, there are reports of a role in cardiomyocyte apoptosis (Gilleron et al. 2009; McLaughlin et al. 2017). There was no difference between the types of fibroblasts or the ACT and DCM patient evident in these data. Our unpublished data in stem cell derived cardiomyocytes show that DOX treatment leads to a higher apoptosis rate, decreased contractile force and higher dysregulation of sarcomeric structure in cardiomyocytes from patients compared to healthy controls.

In summary, this study suggests that cardiac fibroblasts contribute to ACT development through the production of NADPH oxidase 2-derived superoxide and hydrogen peroxide linking the fibroblasts to pathways of cardiac damage, which so far have only been described in cardiomyocytes or whole cardiac tissue. It may be of interest to investigate how superoxide and hydrogen peroxide affect cardiac fibroblasts specifically as ROS-mediated damage has preliminarily only been described for cardiomyocytes. Additionally, the data suggest a higher sensitivity of cardiac fibroblasts from ACT patients, which should be assessed in future research.

4.6 Limitations

The generalisability of the findings from this study are in part restricted by a few limiting factors, which in future research building on the data should be addressed and resolved.

First of all, the study was performed with a small number of patients, due to the difficulties of recruiting fresh left ventricle tissue from ACT patients in particular. While this is also a strength of the study, as insights into human cells is limited, the use of human cardiac material also leads to a shortness of patients. With a small sample size, hampering factors such as the diverging genetic background cannot be dismissed as influencing the results found in this study. As more material is obtained, the experiments should be repeated with more fibroblasts and tissue, reducing the effect of unknown genetic variations.

Another problem is the cultivation of human cardiac fibroblasts *in vitro*. As described in 1.2.1, cardiac fibroblasts transform into the more active myofibroblasts once in culture, similar to the reaction to different forms of cardiac stress in vivo. Therefore, the activated state of the cardiac fibroblasts in this study may attenuate the stress response found with anthracycline treatment. However, this disturbance should not deteriorate the comparison between the different fibroblast groups, as they were cultivated in the same way.

Lastly, the study of isolated cardiac fibroblasts has drawbacks of its own. The myocardium is a complex construct consisting of different cardiomyocytes, fibroblasts, extracellular matrix, nerves and blood vessels. The interaction of cell types with each other and their surroundings is an aspect of homeostasis and pathology that is not represented in this study and may be important for understanding the consequences of the increased ROS production reported by this investigation.

4.7 Future perspectives

Research building on this study could be focused on functional consequences resulting from the increased ROS production in human cardiac fibroblasts. Possible directions with interesting implications might be protein synthesis capacity, Ca^{2+}handling in cardiac fibroblasts and mitochondrial functionality. Especially the regulation and production of the extracellular matrix upon anthracycline treatment may be an interesting topic of future research.

Also, the interaction of cardiac fibroblasts and cardiomyocytes in ACT should be investigated. The use of the 3D-engineered heart muscle platform for functional experiments with induced stem cell-derived cardiomyocytes and the cardiac fibroblasts

appears as a promising tool, because the measurement of cardiac function could be performed with different combinations of diseased and healthy fibroblasts and cardiomyocytes. This would allow conclusions about the contribution of the different cell types to the end result of cardiac dysfunction.

Lastly, the functional consequences of ACT-associated SNPs in the NADPH oxidase subunits need further investigation to unravel potentially predisposing mechanisms. Genetic modification in the induced stem cell-derived cardiomyocytes with CRISPR/Cas might be suitable.

4.8 Conclusion

In the first part of the study, proliferating cells were successfully isolated from fresh cardiac tissue and characterized as cardiac fibroblasts for ACT research. By combining morphology, proliferation and analysis of markers such as *POSTN* and *TCF-21,* a promising protocol for the distinguishing of cardiac fibroblasts against other types of fibroblasts and cardiomyocytes has been established.

When exposed to anthracycline treatment, the cardiac fibroblasts reacted with an increase in the production of ROS and tendencies of expression changes of the NADPH oxidase subunits. Especially the increase in superoxide levels and *NOX2* expression is likely linked. These findings suggest that cardiac fibroblasts contribute to ACT development themself and not only to the manifestation of the fibrotic phenotype following cardiomyocyte apoptosis. Differences between cardiac fibroblasts and skin fibroblasts were found for hydrogen peroxide production and the expression of certain NADPH oxidase subunits supporting the working hypothesis of a distinct role of cardiac fibroblasts in ACT-linked pathomechanisms. The other working hypothesis that ACT cardiac fibroblasts are more sensitive to anthracycline treatment was only found in the hydrogen peroxide measurements, but not in the other experiments.

The NADPH oxidase subunit expression was analyzed in cardiac fibroblasts as an acute reaction and in whole cardiac tissue for chronic ACT. Differences between the ACT patients, DCM patients and healthy controls endorse the enzyme as a promising target for ACT research, especially in the context of functional consequences of anthracycline treatment and ACT-associated SNPs.

5 Summary

A momentous side-effect of the treatment with anthracyclines like doxorubicin (DOX) is the cumulative, dose-dependent damage of the heart. The chronic anthracycline-induced cardiotoxicity (ACT) leads to the development of symptomatic heart failure in 6 to 9 % of all patients treated and is greatly impairing patient outcome. The search for preventive and therapeutic strategies has yielded little success so far as molecular mechanisms are not fully understood. The production of reactive oxygen species (ROS), mitochondrial dysfunction and topoisomerase 2β inhibition have been proposed as parts of the complex and multifactorial disease model. The aim of this study was to investigate the potential role of cardiac fibroblasts in ACT development in terms of ROS production and NAPDH oxidase subunit expression.

Human cardiac fibroblasts (cFB) were isolated from fresh cardiac tissue after heart transplantation from an ACT and a dilative cardiomyopathy (DCM) patient. Isolated cFBs show morphological characteristics, high proliferation capacity and expression of typical cardiac fibroblast markers as periostin, transcription factor 21 and α-smooth muscle actin in qRT-PCR and immunocytochemistry experiments.

To analyze the acute reaction to anthracycline treatment, cFBs were exposed to 0.1 or 0.25 μM DOX for 24 hours and analyzed regarding the expression of NADPH oxidase subunits on mRNA level via qRT-PCR and on protein level via Western blot. Subunits *RAC2* and *NCF4* were expressed significantly more highly in cardiac fibroblasts compared to skin fibroblasts. As an immediate response to DOX treatment, tendencies of expression changes were found for *NOX2*, *NOX4*, *RAC2* and *NCF4*. Additionally, the expression of NADPH oxidase subunits in tissue of chronic heart failure patients was studied showing that expression levels for the subunits differed between ACT patients, DCM patients and healthy controls.

DOX-dependent production of ROS in cFBs was assessed using the Amplex Red reagent for hydrogen peroxide and DHE-HPLC for superoxide. DOX concentrations of 0.1 to 0.25 μM DOX caused a dose-dependent significant increase of ROS. Also, hydrogen peroxide levels were higher in cardiac fibroblasts compared to skin fibroblasts and NADPH-contributable superoxide production was only measurable when the cells were triggered with DOX treatment.

In conclusion, this study suggests that cardiac fibroblasts contribute to ACT development and not only to the manifestation of the fibrotic phenotype following cardiomyocyte apoptosis. Also, the NADPH oxidase appears to be a promising target for further research based on the expression changes and differences found in this study.

6 Appendix

Table A1: Mean CT-values of qRT-PCR experiments for fibroblast characterization (Figure 9)

Gene	Mean CT-value
COL1	20,1
FSP-1	21,83
GAPDH	18,46
POSTN	23,47
TCF21	25,62
a-SMA	21,21

Table A2: Mean CT-values of qRT-PCR experiments for cardiac and skin fibroblasts (Figure 12)

Gene	Mean CT-value
CYBA	22,16
GAPDH	18,64
NCF4	34,12
NOX2	34,62
NOX4	29,46
RAC1	21,7
RAC2	25,64

Table A3: Mean CT-values of qRT-PCR experiments for cardiac tissue (Figure 15)

Gene	Mean CT-value
CYBA	28,48
GAPDH	18,03
NCF1	32,21
NCF2	34,5
NCF4	30,11
NOX2	29,48
NOX4	30,09
RAC1	23,15
RAC2	30,41

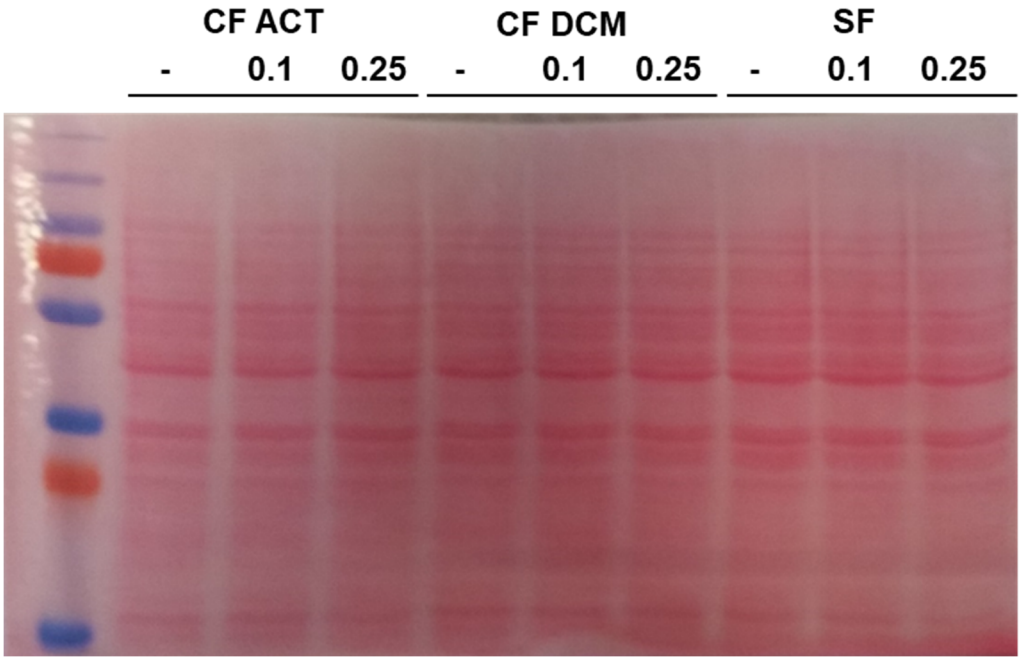

Figure A1: Ponceau red staining of the western blot experiments for cardiac and skin fibroblasts (Figure 14)

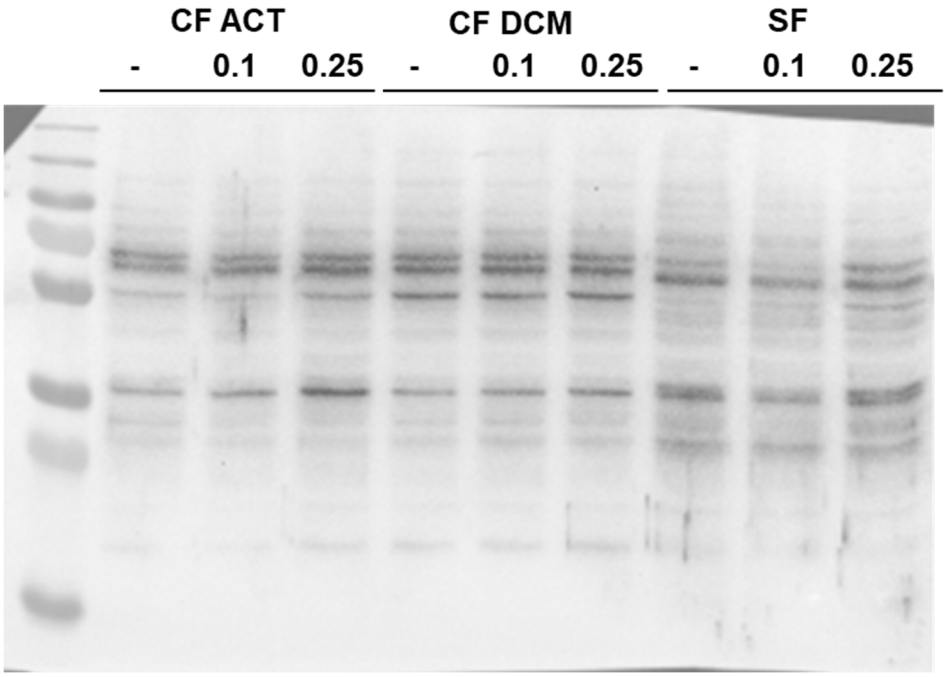

Figure A2: Protein expression of NOX4 in human fibroblasts. Full western blot image from Figure 14.

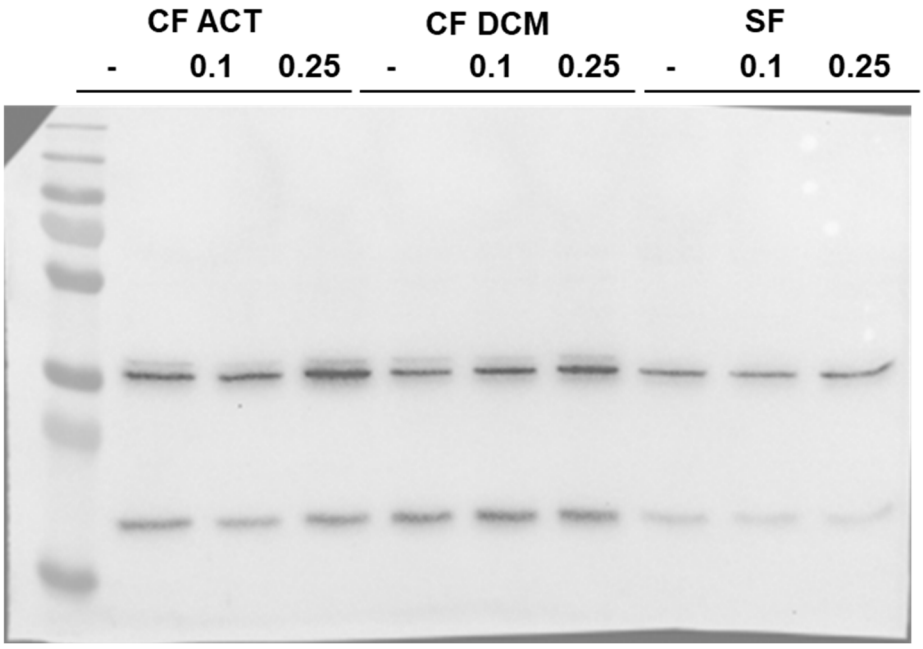

Figure A3: Protein expression of RAC2 in human fibroblasts. Full western blot image from Figure 14.

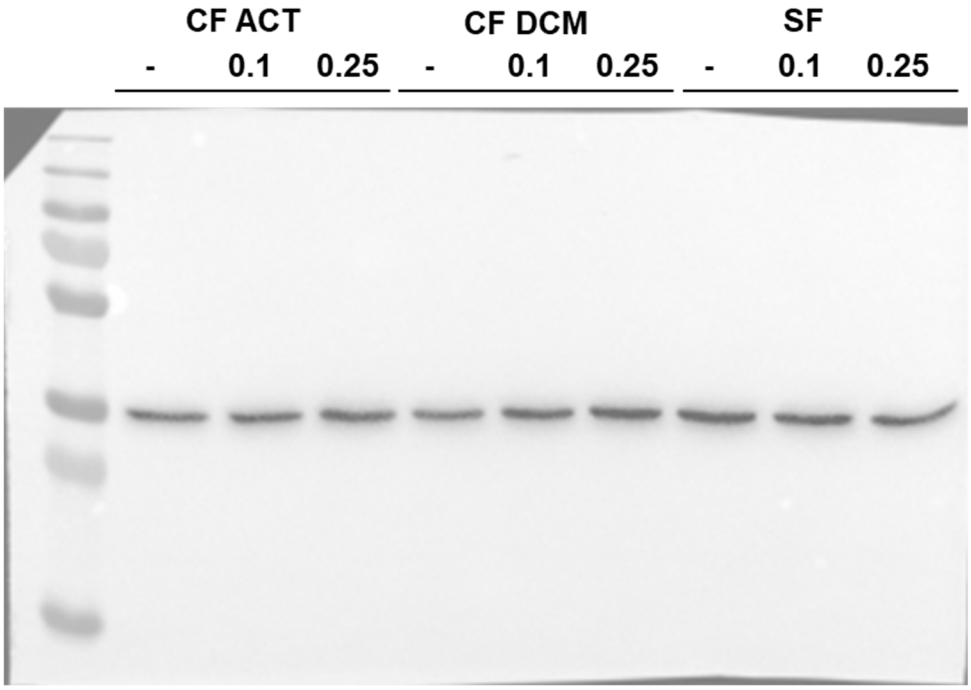

Figure A4: Protein expression of GAPDH in human fibroblasts. Full western blot image from Figure 14.

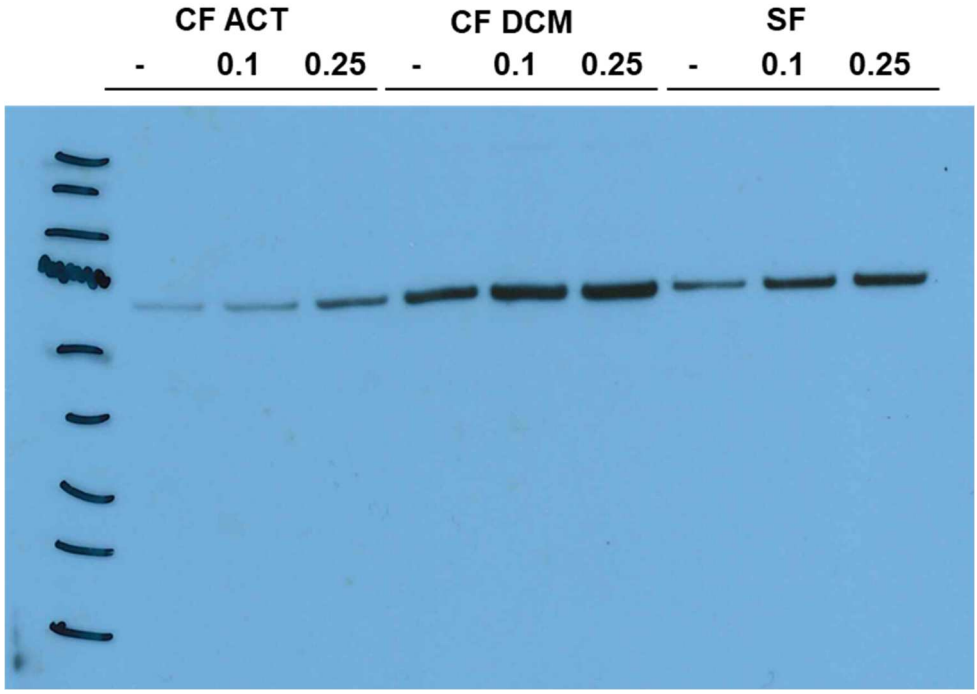

Figure A5: Protein expression of NOX2 in the membrane fraction of human fibroblasts. Full western blot image from Figure 13.

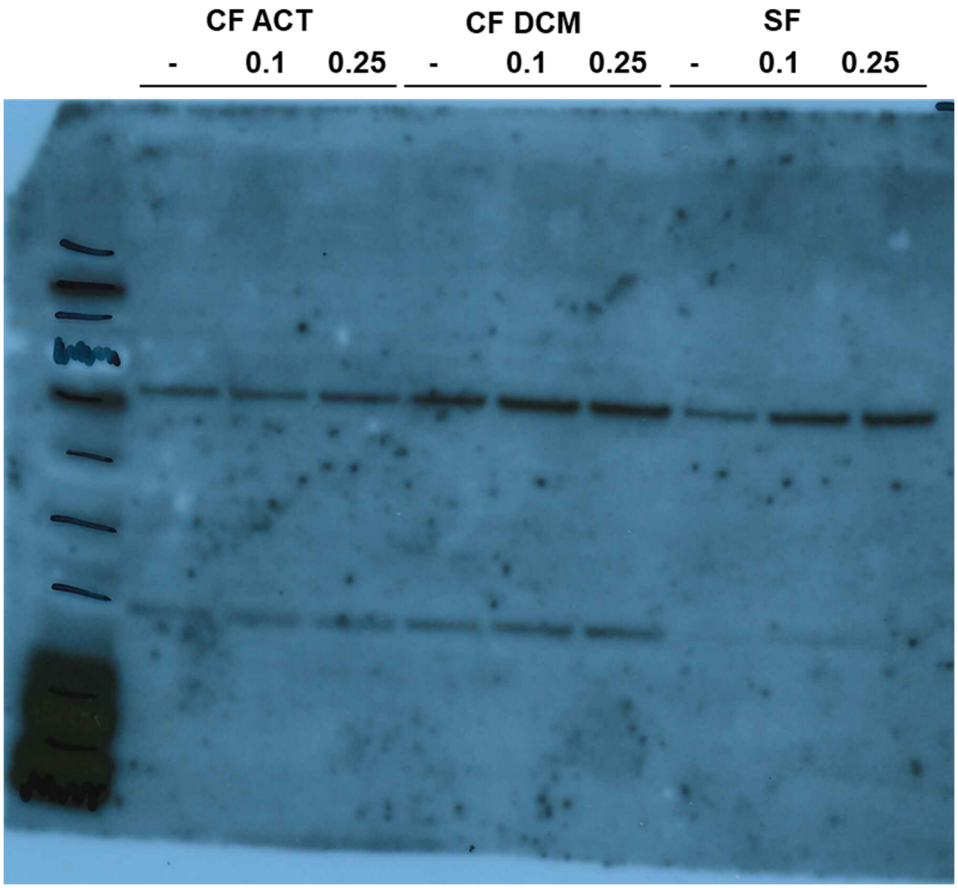

Figure A6: Protein expression of p22 in the membrane fraction of human fibroblasts. Full western blot image from Figure 13.

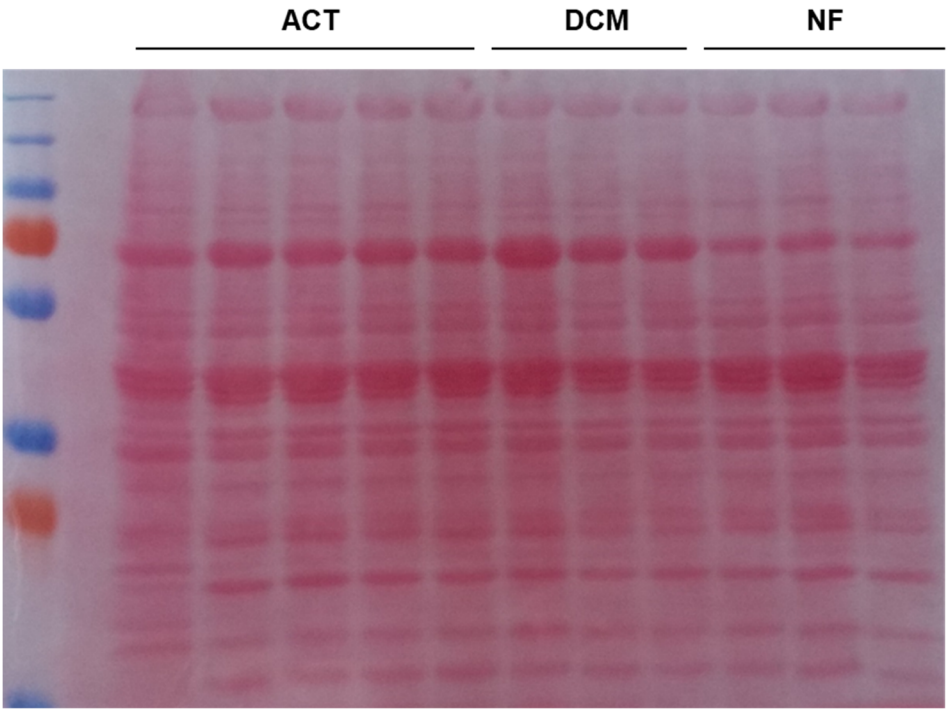

Figure A7: Ponceau red staining of the western blot experiments for cardiac tissue (Figure 16)

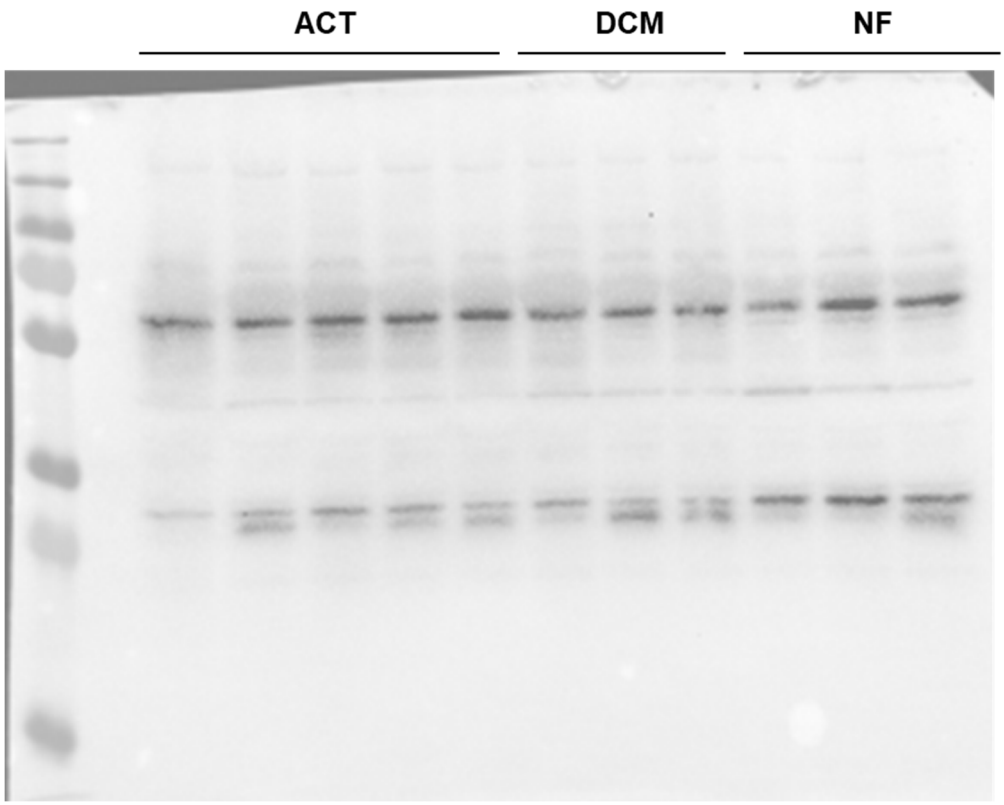

Figure A8: Protein expression of NOX4 in human cardiac tissue. Full western blot image from Figure 16.

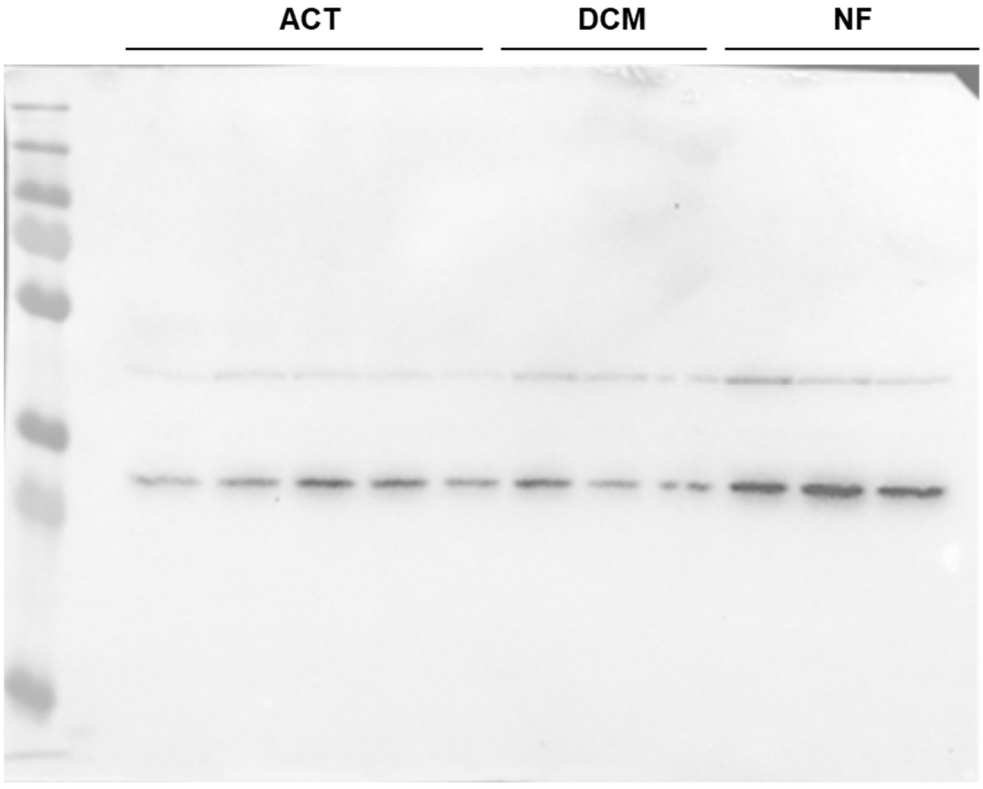

Figure A9: Protein expression of RAC2 in human cardiac tissue. Full western blot image from Figure 16.

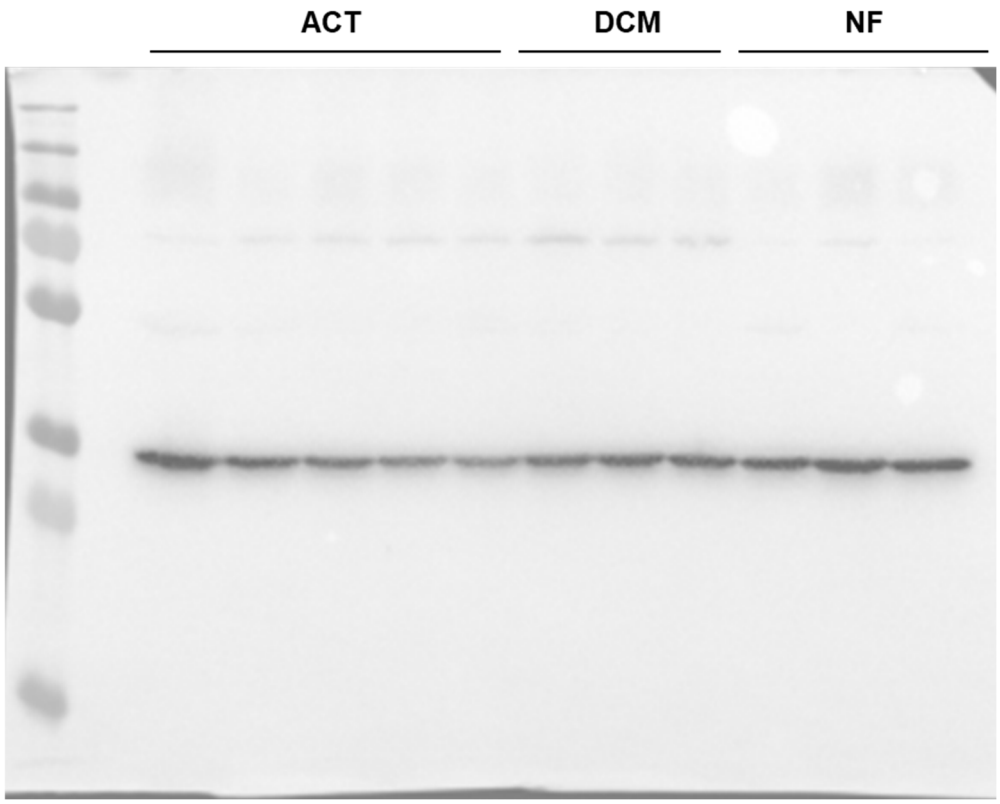

Figure A10: Protein expression of GAPDH in human cardiac tissue. Full western blot image from Figure 16.

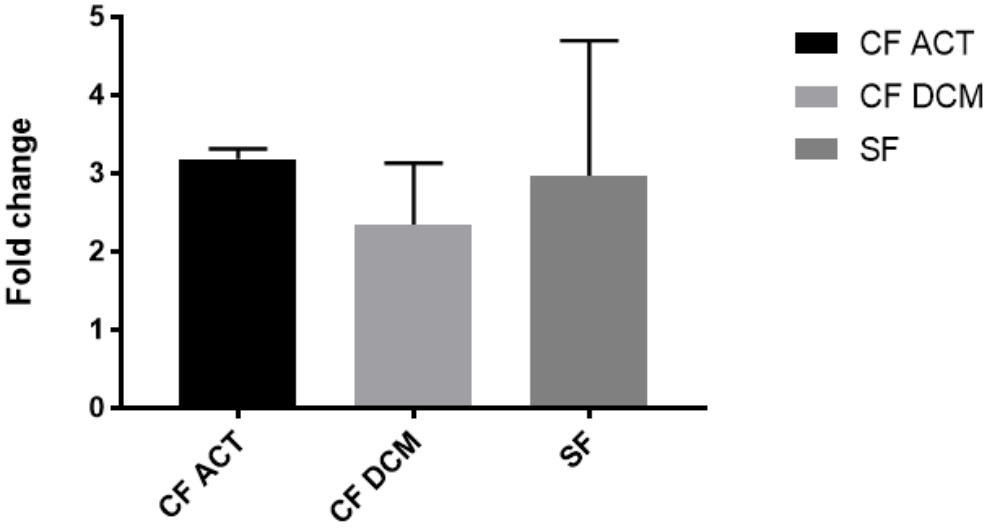

Figure A11: Fold change in superoxide production from basal level to 0.25µM DOX in membrane fractions of ACT-4 cardiac fibroblasts (CF ACT), DCM-1 cardiac fibroblasts (CF DCM) and skin fibroblasts from DCM-1 (SF) n=2 biological replicates for each measurement.

7 References

Anderson KR, Sutton M. G. St J., Lie J. T. (1979): Histopathological types of cardiac fibrosis in myocardial disease. J Pathol 128, 79–85

Angelis AD, Piegari E, Cappetta D, Marino L, Filippelli A, Berrino L, Ferreira-Martins J, Zheng H, Hosoda T, Rota M, et al. (2010): Anthracycline Cardiomyopathy Is Mediated by Depletion of the Cardiac Stem Cell Pool and Is Rescued by Restoration of Progenitor Cell Function. Circulation 121, 276–292

Arcamone F, Cassinelli G, Fantini G, Grein A, Orezzi P, Pol C, Spalla C (1969): Adriamycin, 14-hydroxydaunomycin, a new antitumor antibiotic from *S. peucetius var.* caesius. Biotechnol Bioeng 11, 1101–1110

Arola OJ, Saraste A, Pulkki K, Kallajoki M, Parvinen M, Voipio-Pulkki L-M (2000): Acute Doxorubicin Cardiotoxicity Involves Cardiomyocyte Apoptosis. Cancer Res 60, 1789–1792

Babior BM (1999): NADPH Oxidase: An Update. Blood 93, 1464–1476

Berthiaume JM, Wallace KB (2007): Adriamycin-induced oxidative mitochondrial cardiotoxicity. Cell Biol Toxicol 23, 15–25

Biberstine-Kinkade KJ, Yu L, Stull N, LeRoy B, Bennett S, Cross A, Dinauer MC (2002): Mutagenesis of p22 phox Histidine 94: A histidine in this position is not required for flavocytochrome b558 function. J Biol Chem 277, 30368–30374

Binaschi M, Bigioni M, Cipollone A, Rossi C, Goso C, Maggi CA, Capranico G, Animati F (2001): Anthracyclines: selected new developments. Curr Med Chem Anti-Cancer Agents 1, 113–130

Brandes RP, Weissmann N, Schröder K (2014): Nox family NADPH oxidases: Molecular mechanisms of activation. Free Radic Biol Med 76, 208–226

Brieger K, Schiavone S, Miller FJJ, Krause K-H (2012): Reactive oxygen species: from health to disease. Swiss Med Wkly 142, w13659

Burridge PW, Li YF, Matsa E, Wu H, Ong S-G, Sharma A, Holmström A, Chang AC, Coronado MJ, Ebert AD, et al. (2016): Human Induced Pluripotent Stem Cell–Derived Cardiomyocytes Recapitulate the Predilection of Breast Cancer Patients to Doxorubicin–Induced Cardiotoxicity. Nat Med 22, 547-556

Cappetta D, Esposito G, Piegari E, Russo R, Ciuffreda LP, Rivellino A, Berrino L, Rossi F, Angelis AD, Urbanek K (2016): SIRT1 activation attenuates diastolic dysfunction by reducing cardiac fibrosis in a model of anthracycline cardiomyopathy. Int J Cardiol 205, 99–110

Cardinale D, Sandri MT, Colombo A, Colombo N, Boeri M, Lamantia G, Civelli M, Peccatori F, Martinelli G, Fiorentini C, Cipolla CM (2004): Prognostic Value of Troponin I in Cardiac Risk Stratification of Cancer Patients Undergoing High-Dose Chemotherapy. Circulation 109, 2749–2754

Cardinale D, Colombo A, Bacchiani G, Tedeschi I, Meroni CA, Veglia F, Civelli M, Lamantia G, Colombo N, Curigliano G, et al. (2015): Early Detection of Anthracycline Cardiotoxicity and Improvement With Heart Failure Therapy clinical perspective. Circulation 131, 1981–1988

Carvalho FS, Burgeiro A, Garcia R, Moreno AJ, Carvalho RA, Oliveira PJ (2014): Doxorubicin-Induced Cardiotoxicity: From Bioenergetic Failure and Cell Death to Cardiomyopathy. Med Res Rev 34, 106–135

Cascales A, Pastor-Quirante F, Sánchez-Vega B, Luengo-Gil G, Corral J, Ortuño-Pacheco G, Vicente V, de la Peña FA (2013): Association of Anthracycline-Related Cardiac Histological Lesions With NADPH Oxidase Functional Polymorphisms. Oncologist 18, 446–453

Cave AC, Brewer AC, Narayanapanicker A, Ray R, Grieve DJ, Walker S, Shah AM (2006): NADPH Oxidases in Cardiovascular Health and Disease. Antioxid Redox Signal 8, 691–728

Chung W-B, Youn H-J (2016): Pathophysiology and preventive strategies of anthracycline-induced cardiotoxicity. Korean J Intern Med 31, 625–633

Coleman M, Forman D, Bryant H, Butler J, Rachet B, Maringe C, Nur U, Tracey E, Coory M, Hatcher J, et al. (2011): Cancer survival in Australia, Canada, Denmark, Norway, Sweden, and the UK, 1995–2007 (the International Cancer Benchmarking Partnership): an analysis of population-based cancer registry data. Lancet 377, 127–138

Cormack DH: Essential Histology 2nd edition; Lippincott Williams & Wilkins, Philadelphia, 2001

Cucoranu I, Clempus R, Dikalova A, Phelan PJ, Ariyan S, Dikalov S, Sorescu D (2005): NAD(P)H Oxidase 4 Mediates Transforming Growth Factor-β1–Induced Differentiation of Cardiac Fibroblasts Into Myofibroblasts. Circ Res 97, 900–907

Daugaard Gedske, Lassen Ulrik, Bie Peter, Pedersen Erling Bjerregaard, Jensen Kaare Troels, Abildgaard Ulrik, Hesse Birger, Kjaer Andreas (2005): Natriuretic peptides in the monitoring of anthracycline induced reduction in left ventricular ejection fraction. Eur J Heart Fail 7, 87–93

Deb A, Ubil E (2014): Cardiac Fibroblast in Development and Wound Healing. J Mol Cell Cardiol 70, 47–55

Demant EJ, Jensen PK (2005): Destruction of Phosphilipids and Respiratory-Chain Activity in Pig=Heart Submitochondrial Particles Induced by an Adriamycin-Iron Complex. Eur J Biochem 132, 551–556

Di S, Marotta M, Salvatore G, Cudemo G, Cuda G, De Vivo F, Di B, Ciaramella F, Caputo G, de Divitiis O (2000): Changes in myocardial cytoskeletal intermediate filaments and myocyte contractile dysfunction in dilated cardiomyopathy: an in vivo study in humans. Heart 84, 659–667

Doroshow JH, Davies KJ (1986): Redox cycling of anthracyclines by cardiac mitochondria. II. Formation of superoxide anion, hydrogen peroxide, and hydroxyl radical. J Biol Chem 261, 3068–3074

Doroshow JH, Locker GY, Myers CE (1980): Enzymatic Defenses of the Mouse Heart Against Reactive Oxygen Metabolites: Alterations produced by doxorubicin. J Clin Invest 65, 128-135

Doroshow JH, Tallent C, Schechter JE (1985): Ultrastructural features of Adriamycin-induced skeletal and cardiac muscle toxicity. Am J Pathol 118, 288–297

Doyle JJ, Neugut AI, Jacobson JS, Grann VR, Hershman DL (2005): Chemotherapy and Cardiotoxicity in Older Breast Cancer Patients: A Population-Based Study. J Clin Oncol 23, 8597–8605

Fan LM, Teng L, Li J-M (2009): Knockout of p47phox Uncovers a Critical Role of p40phox in Reactive Oxygen Species Production in Microvascular Endothelial Cells. Arterioscler Thromb Vasc Biol 29, 1651–1656

Finck BN, Kelly DP (2007): Peroxisome Proliferator–Activated Receptor γ Coactivator-1 (PGC-1) Regulatory Cascade in Cardiac Physiology and Disease. Circulation 115, 2540–2548

Fink B, Laude K, McCann L, Doughan A, Harrison DG, Dikalov S (2004): Detection of intracellular superoxide formation in endothelial cells and intact tissues using dihydroethidium and an HPLC-based assay. Am J Physiol Cell Physiol 287, C895-902

Fu LX, Waagstein F, Hjalmarson Å (1990): A new insight into adriamycin-induced cardiotoxicity. Int J Cardiol 29, 15–20

Ganz WI, Sridhar KS, Forness TJ (1993): Detection of early anthracycline cardiotoxicity by monitoring the peak filling rate. Am J Clin Oncol 16, 109–112

Gaudin PB, Hruban RH, Beschorner WE, Kasper EK, Olson JL, Baughman KL, Hutchins GM (1993): Myocarditis associated with doxorubicin cardiotoxicity. Am J Clin Pathol 100, 158–163

Gewirtz D (1999): A critical evaluation of the mechanisms of action proposed for the antitumor effects of the anthracycline antibiotics adriamycin and daunorubicin. Biochem Pharmacol 57, 727–741

Gilleron M, Marechal X, Montaigne D, Franczak J, Neviere R, Lancel S (2009): NADPH oxidases participate to doxorubicin-induced cardiac myocyte apoptosis. Biochem Biophys Res Commun 388, 727–731

Guglin M, Aljayeh M, Saiyad S, Ali R, Curtis AB (2009): Introducing a new entity: chemotherapy-induced arrhythmia. EP Europace 11, 1579–1586

Guzik TJ, West NEJ, Black E, McDonald D, Ratnatunga C, Pillai R, Channon KM (2000): Functional Effect of the C242T Polymorphism in the NAD(P)H Oxidase p22phox Gene on Vascular Superoxide Production in Atherosclerosis. Circulation 102, 1744–1747

Haupt L: Modeling anthracycline-induced cardiotoxicity with patient-specific iPSCs. Biol. Diss. 2018

Hayashi H, Kobara M, Abe M, Tanaka N, Gouda E, Toba H, Yamada H, Tatsumi T, Nakata T, Matsubara H (2008): Aldosterone Nongenomically Produces NADPH Oxidase–Dependent Reactive Oxygen Species and Induces Myocyte Apoptosis. Hypertens Res 31, 363-375

Ichihara S, Yamada Y, Kawai Y, Osawa T, Furuhashi K, Duan Z, Ichihara G (2007): Roles of oxidative stress and Akt signaling in doxorubicin cardiotoxicity. Biochem Biophys Res Commun 359, 27–33

Johar S, Cave AC, Narayanapanicker A, Grieve DJ, Shah AM (2006): Aldosterone mediates angiotensin II-induced interstitial cardiac fibrosis via a Nox2-containing NADPH oxidase. FASEB J 20, 1546–1548

Kaiserová H, Šimůnek T, Štěrba M, Hartog GJM den, Schröterová L, Popelová O, Geršl V, Kvasničková E, Bast A (2007): New iron chelators in anthracycline-induced cardiotoxicity. Cardiovasc Toxicol 7, 145–150

Kanisicak O, Khalil H, Ivey MJ, Karch J, Maliken BD, Correll RN, Brody MJ, J Lin S-C, Aronow BJ, Tallquist MD, Molkentin JD (2016): Genetic lineage tracing defines myofibroblast origin and function in the injured heart. Nat Commun 7, 12260

Kaur H, Takefuji M, Ngai CY, Carvalho J, Bayer J, Wietelmann A, Poetsch A, Hoelper S, Conway SJ, Möllmann H, et al. (2016): Targeted Ablation of Periostin-Expressing Activated Fibroblasts Prevents Adverse Cardiac Remodeling in MiceNovelty and Significance. Circ Res 118, 1906–1917

Khiati S, Rosa ID, Sourbier C, Ma X, Rao VA, Neckers LM, Zhang H, Pommier Y (2014): Mitochondrial Topoisomerase I (Top1mt) Is a Novel Limiting Factor of Doxorubicin Cardiotoxicity. Clin Cancer Res 20, 4873–4881

Kilickap S, Akgul E, Aksoy S, Aytemir K, Barista I (2005): Doxorubicin-induced second degree and complete atrioventricular block. EP Europace 7, 227–230

Kremer LCM, van Dalen EC, Offringa M, Voûte PA (2002): Frequency and risk factors of anthracycline-induced clinical heart failure in children: a systematic review. Ann Oncol 13, 503–512

Krenning G, Zeisberg EM, Kalluri R (2010): The Origin of Fibroblasts and Mechanism of Cardiac Fibrosis. J Cell Physiol 225, 631

Kuroda J, Sadoshima J (2010): NADPH Oxidase and Cardiac Failure. J Cardiovasc Transl Res 3, 314–320

Lassègue B, Martín AS, Griendling KK (2012): Biochemistry, Physiology, and Pathophysiology of NADPH Oxidases in the Cardiovascular System. Circ Res 110, 1364–1390

Laurindo FRM, Fernandes DC, Santos CXC (2008): Assessment of superoxide production and NADPH oxidase activity by HPLC analysis of dihydroethidium oxidation products. Methods Enzymol 441, 237–260

Leask A (2015): Getting to the Heart of the Matter: New Insights Into Cardiac Fibrosis. Circ Res 116, 1269–1276

Lebrecht D, Kokkori Aikaterini, Ketelsen Uwe-Peter, Setzer Bernhard, Walker Ulrich (2005): Tissue-specific mtDNA lesions and radical-associated mitochondrial dysfunction in human hearts exposed to doxorubicin. J Pathol 207, 436–444

L'Ecuyer T, Sanjeev S, Thomas R, Novak R, Das L, Campbell W, Heide RV (2006): DNA damage is an early event in doxorubicin-induced cardiac myocyte death. Am J Physiol Heart Circ Physiol 291, H1273–H1280

Leong SL, Chaiyakunapruk N, Lee SWH (2017): Candidate Gene Association Studies of Anthracycline-induced Cardiotoxicity: A Systematic Review and Meta-analysis. Sci Rep 7, 39

Leslie KO, Taatjes DJ, Schwarz J, vonTurkovich M, Low RB (1991): Cardiac myofibroblasts express alpha smooth muscle actin during right ventricular pressure overload in the rabbit. Am J Pathol 139, 207

Lim CC, Zuppinger C, Guo X, Kuster GM, Helmes M, Eppenberger HM, Suter TM, Liao R, Sawyer DB (2004): Anthracyclines Induce Calpain-dependent Titin Proteolysis and Necrosis in Cardiomyocytes. J Biol Chem 279, 8290–8299

Lipshultz SE, Scully RE, Lipsitz SR, Sallan SE, Silverman LB, Miller TL, Barry EV, Asselin BL, Athale U, Clavell LA, et al. (2010): Assessment of dexrazoxane as a cardioprotectant in doxorubicin-treated children with high-risk acute lymphoblastic leukaemia: long-term follow-up of a prospective, randomised, multicentre trial. Lancet Oncol 11, 950–961

Lopes LR, Dagher M-C, Gutierrez A, Young B, Bouin A-P, Fuchs A, Babior BM (2004): Phosphorylated p40PHOX as a Negative Regulator of NADPH Oxidase. Biochemistry 43, 3723–3730

Lotrionte M, Biondi-Zoccai G, Abbate A, Lanzetta G, D'Ascenzo F, Malavasi V, Peruzzi M, Frati G, Palazzoni G (2013): Review and Meta-Analysis of Incidence and Clinical Predictors of Anthracycline Cardiotoxicity. Am J Cardiol 112, 1980–1984

Lyu YL, Kerrigan JE, Lin C-P, Azarova AM, Tsai Y-C, Ban Y, Liu LF (2007): Topoisomerase IIβ–Mediated DNA Double-Strand Breaks: Implications in Doxorubicin Cardiotoxicity and Prevention by Dexrazoxane. Cancer Res 67, 8839–8846

Ma J, Wang Y, Zheng D, Wei M, Xu H, Peng T (2013): Rac1 signalling mediates doxorubicin-induced cardiotoxicity through both reactive oxygen species-dependent and -independent pathways. Cardiovasc Res 97, 77–87

Maack C, Kartes T, Kilter H, Schäfers H-J, Nickenig G, Böhm M, Laufs U (2003): Oxygen Free Radical Release in Human Failing Myocardium Is Associated With Increased Activity of Rac1-GTPase and Represents a Target for Statin Treatment. Circulation 108, 1567–1574

Martin ML, Blaxall BC (2012): Cardiac intercellular communication: are myocytes and fibroblasts fair-weather friends? J Cardiovasc Transl Res 5, 768–782

Martyn KD, Frederick LM, von Loehneysen K, Dinauer MC, Knaus UG (2006): Functional analysis of Nox4 reveals unique characteristics compared to other NADPH oxidases. Cell Signal 18, 69–82

McGowan JV, Chung R, Maulik A, Piotrowska I, Walker JM, Yellon DM (2017): Anthracycline Chemotherapy and Cardiotoxicity. Cardiovasc Drugs Ther 31, 63–75

McLaughlin D, Zhao Y, O'Neill KM, Edgar KS, Dunne PD, Kearney AM, Grieve DJ, McDermott BJ (2017): Signalling mechanisms underlying doxorubicin and Nox2 NADPH oxidase-induced cardiomyopathy: involvement of mitofusin-2. Br J Pharmacol 174, 3677

Middleman E, Luce J, Frei E (1971): Clinical trials with adriamycin. Cancer 28, 844–850

Minotti G, Menna P, Salvatorelli E, Cairo G, Gianni L (2004): Anthracyclines: Molecular Advances and Pharmacologic Developments in Antitumor Activity and Cardiotoxicity. Pharmacol Rev 56, 185–229

Nitiss KC, Nitiss JL (2014): Twisting and Ironing: Doxorubicin Cardiotoxicity by Mitochondrial DNA Damage. Clin Cancer Res 20, 4737–4739

Nozaki N, Shishido T, Takeishi Y, Kubota I (2004): Modulation of Doxorubicin-Induced Cardiac Dysfunction in Toll-Like Receptor-2–Knockout Mice. Circulation 110, 2869–2874

Ondrias K, Borgatta L, Kim DH, Ehrlich BE (1990): Biphasic effects of doxorubicin on the calcium release channel from sarcoplasmic reticulum of cardiac muscle. Circ Res 67, 1167–1174

Porter KE, Turner NA (2009): Cardiac fibroblasts: At the heart of myocardial remodeling. Pharmacol Ther 123, 255–278

Rahman AM, Yusuf SW, Ewer MS (2007): Anthracycline-induced cardiotoxicity and the cardiac-sparing effect of liposomal formulation. Int J Nanomedicine 2, 567–583

Reichwagen A, Ziepert M, Kreuz M, Gödtel-Armbrust U, Rixecker T, Poeschel V, Reza Toliat M, Nürnberg P, Tzvetkov M, Deng S, et al. (2015): Association of NADPH oxidase

polymorphisms with anthracycline-induced cardiotoxicity in the RICOVER-60 trial of patients with aggressive CD20+ B-cell lymphoma. Pharmacogenomics 16, 361–372

Rotrosen D, Yeung CL, Leto TL, Malech HL, Kwong CH (1992): Cytochrome b558: the flavin-binding component of the phagocyte NADPH oxidase. Science 256, 1459–1462

Saeki K, Obi I, Ogiku N, Shigekawa M, Imagawa T, Matsumoto T (2002): Doxorubicin directly binds to the cardiac-type ryanodine receptor. Life Sci 70, 2377–2389

Schirmer M, Hoffmann M, Kaya E, Tzvetkov M, Brockmöller J (2008): Genetic polymorphisms of NAD(P)H oxidase: variation in subunit expression and enzyme activity. Pharmacogenomics J 8, 297–304

Shimo-Nakanishi Y, Hasebe T, Suzuki A, Mochizuki H, Nomiyama T, Tanaka Y, Nagaoka I, Mizuno Y, Urabe T (2004): Functional effects of NAD(P)H oxidase p22phox C242T mutation in human leukocytes and association with thrombotic cerebral infarction. Atherosclerosis 175, 109–115

Siegel RL, Miller KD, Jemal A (2018): Cancer statistics, 2018. CA Cancer J Clin 68, 7–30

Singal PK (1998): Doxorubicin-induced cardiomyopathy. N Engl J Med 339, 900–905

Steinherz LJ, Steinherz PG, Tan CT, Heller G, Murphy ML (1991): Cardiac toxicity 4 to 20 years after completing anthracycline therapy. JAMA 266, 1672-1677

Strutz F, Okada H, Lo CW, Danoff T, Carone RL, Tomaszewski JE, Neilson EG (1995): Identification and characterization of a fibroblast marker: FSP1. J Cell Biol 130, 393–405

Swain, Whaley Fredrick S., Ewer Michael S. (2003): Congestive heart failure in patients treated with doxorubicin. Cancer 97, 2869–2879

Tamene AM, Masri C, Konety SH (2015): Cardiovascular MR Imaging in Cardio-oncology. Magn Reson Imaging Clin N Am 23, 105–116

Tan TC, Neilan TG, Francis S, Plana JC, Scherrer-Crosbie M (2015): Anthracycline-Induced Cardiomyopathy in Adults. Compr Physiol 5, 1517–1540

Tewey KM, Rowe TC, Yang L, Halligan BD, Liu LF (1984): Adriamycin-induced DNA damage mediated by mammalian DNA topoisomerase II. Science 226, 466–468

Thavendiranathan P, Poulin F, Lim K-D, Plana JC, Woo A, Marwick TH (2014): Use of Myocardial Strain Imaging by Echocardiography for the Early Detection of Cardiotoxicity in Patients During and After Cancer Chemotherapy: A Systematic Review. J Am Coll Cardiol 63, 2751–2768

Thornalley PJ, Dodd NJF (1985): Free radical production from normal and adriamycin-treated rat cardiac sarcosomes. Biochem Pharmacol 34, 669–674

Tokarska-Schlattner M, Zaugg M, Zuppinger C, Wallimann T, Schlattner U (2006): New insights into doxorubicin-induced cardiotoxicity: The critical role of cellular energetics. J Mol Cell Cardiol 41, 389–405

Unverferth DV, Fetters JK, Unverferth BJ, Leier CV, Magorien RD, Arn AR, Baker PB (1983): Human myocardial histologic characteristics in congestive heart failure. Circulation 68, 1194–1200

van Dalen EC, Caron HN, Dickinson HO, Kremer LC (2011): Cardioprotective interventions for cancer patients receiving anthracyclines. Cochrane Database Syst Rev 2011, CD003917

van Nieuwenhoven FA, Turner NA (2013): The role of cardiac fibroblasts in the transition from inflammation to fibrosis following myocardial infarction. Vascul Pharmacol 58, 182–188

Vásquez-Vivar J, Martasek P, Hogg N, Masters BSS, Pritchard Kirkwood A, Kalyanaraman B (1997): Endothelial Nitric Oxide Synthase-Dependent Superoxide Generation from Adriamycin. Biochemistry 36, 11293–11297

Von Hoff DD (1979): Risk Factors for Doxorubicin-lnduced Congestive Heart Failure. Ann Intern Med 91, 710-717

Wang JC (2002): Cellular roles of DNA topoisomerases: a molecular perspective. Nat Rev Mol Cell Biol 3, 430-440

Weber KT, Sun Y, Bhattacharya SK, Ahokas RA, Gerling IC (2013): Myofibroblast-mediated mechanisms of pathological remodelling of the heart. Nat Rev Cardiol 10, 15-26

Wojnowski L, Kulle B, Schirmer M, Schlüter G, Schmidt A, Rosenberger A, Vonhof S, Bickeböller H, Toliat MR, Suk E-K, et al. (2005): NAD(P)H Oxidase and Multidrug Resistance Protein Genetic Polymorphisms Are Associated With Doxorubicin-Induced Cardiotoxicity. Circulation 112, 3754–3762

World Health Organization: WHO Model List of Essential Medicines. WHO, Genf 2017

Yancy CW, Jessup M, Bozkurt B, Butler J, Casey DE, Drazner MH, Fonarow GC, Geraci SA, Horwich T, Januzzi JL, et al. (2013): 2013 ACCF/AHA Guideline for the Management of Heart Failure: A Report of the American College of Cardiology Foundation/American Heart Association Task Force on Practice Guidelines. J Am Coll Cardiol 62, e147–e239

Zeisberg EM, Tarnavski O, Zeisberg M, Dorfman AL, McMullen JR, Gustafsson E, Chandraker A, Yuan X, Pu WT, Roberts AB, et al. (2007): Endothelial-to-mesenchymal transition contributes to cardiac fibrosis. Nat Med 13, 952–961

Zhan H, Aizawa K, Sun J, Tomida S, Otsu K, Conway SJ, Mckinnon PJ, Manabe I, Komuro I, Miyagawa K, et al. (2016): Ataxia telangiectasia mutated in cardiac fibroblasts regulates doxorubicin-induced cardiotoxicity. Cardiovasc Res 110, 85–95

Zhang M, Brewer AC, Schröder K, Santos CXC, Grieve DJ, Wang M, Anilkumar N, Yu B, Dong X, Walker SJ, et al. (2010): NADPH oxidase-4 mediates protection against chronic load-induced stress in mouse hearts by enhancing angiogenesis. Proc Natl Acad Sci U S A 107, 18121-18126

Zhang M, Perino A, Ghigo A, Hirsch E, Shah AM (2013): NADPH Oxidases in Heart Failure: Poachers or Gamekeepers? Antioxid Redox Signal 18, 1024-1041

Zhang S, Liu X, Bawa-Khalfe T, Lu L-S, Lyu YL, Liu LF, Yeh ETH (2012): Identification of the molecular basis of doxorubicin-induced cardiotoxicity. Nat Med 18, 1639

Zhang W, Clair DS, Butterfield A, Vore M (2016): Loss of Mrp1 Potentiates Doxorubicin-Induced Cytotoxicity in Neonatal Mouse Cardiomyocytes and Cardiac Fibroblasts. Toxicol Sci 151, 44

Zhao H, Kalivendi S, Zhang H, Joseph J, Nithipatikom K, Vásquez-Vivar J, Kalyanaraman B (2003): Superoxide reacts with hydroethidine but forms a fluorescent product that is distinctly different from ethidium: potential implications in intracellular fluorescence detection of superoxide. Free Radic Biol Med 34, 1359–1368-1645

Zhao Y, McLaughlin D, Robinson E, Harvey AP, Hookham MB, Shah AM, McDermott BJ, Grieve DJ (2010): Nox2 NADPH Oxidase Promotes Pathologic Cardiac Remodeling Associated with Doxorubicin Chemotherapy. Cancer Res 70, 9287–9297

Danksagung

Ich möchte meinen tief verbundenen Dank für die Unterstützung bei der Erstellung dieser Dissertationsschrift ausdrücken.

Mein Dank geht an die anonymen Patientinnen und Patienten, die nach überstandener Krebserkrankung, Chemotherapie und/oder Herzinsuffizienz bereit waren Herz- und Hautgewebe an die medizinische Forschung zu spenden.

Außerdem möchte ich mich bei meiner Doktormutter und Betreuerin Frau PD Dr. Katrin Streckfuß-Bömeke für das Vertrauen und die Unterstützung der vergangenen Jahre bedanken. Ebenfalls gilt mein Dank meinem Zweitbetreuer Herrn Prof. Dr. Thomas Meyer sowie Herrn Prof. Dr. Ajay Shah und Dr. Celio Santos für die Gastfreundschaft und wissenschaftliche Hilfe bei meinem Aufenthalt am King's College London. Ermöglicht wurde mir der Aufenthalt durch das IRTG 1816. Für die wissenschaftliche und finanzielle Unterstützung des IRTG 1816 und des Deutschen Zentrums für Herz-Kreislauf-Forschung möchte ich mich bedanken.

Ebenso möchte ich mich bei Frau Dr. Gertrude Bunt, Dr. Andre Sasse und Dr. Hanibal Bohnenberger für die Hilfe bei der Färbung und Mikroskopie der kardialen Schnitte bedanken.

Nicht zuletzt gilt mein Dank der gesamten Arbeitsgruppe Streckfuß-Bömeke. Von der Einarbeitung bis zur abschließenden Schreibarbeit drei Jahre später möchte ich für die Unterstützung meinen Dank ausdrücken. Vielen Dank an Sandra Georgi, Carmen Klopper, Johanna Heine, Sabine Rebs, Luis Haupt, Thomas Borchert, Andreas Maus, Dr. Daniela Hübscher, Celina Guessoum und Maximilian Karls.